



When and why microbial-explicit soil organic carbon models can be unstable

Erik Schwarz¹, Samia Ghersheen², Salim Belyazid¹, and Stefano Manzoni¹

¹Department of Physical Geography and Bolin Centre for Climate Research, Stockholm University, Stockholm, Sweden

²Department of Soil and Environment, Swedish University of Agricultural Sciences, Uppsala, Sweden

Correspondence: Erik Schwarz (erik.schwarz@natgeo.su.se)

Abstract. Microbial-explicit soil organic carbon (SOC) cycling models are increasingly recognized for their advantages over linear models in describing SOC dynamics. These models are known to exhibit oscillations, but it is not clear when they yield stable vs. unstable equilibrium points (EPs) – i.e. EPs that exist analytically, but are not stable to small perturbations and cannot be reached by transient simulations. Occurrence of such unstable EPs can lead to unexpected model behaviour in transient simulations or unrealistic predictions of steady state soil organic carbon (SOC) stocks. Here we ask when and why unstable EPs can occur in an archetypal microbial-explicit model (representing SOC, dissolved OC [DOC], microbial biomass, and extracellular enzymes) and some simplified versions of it. Further, if a model formulation allows for physically meaningful but unstable EPs, can we find constraints in the model parameters (i.e. environmental conditions and microbial traits) that ensure stability of the EPs? We use analytical, numerical and descriptive tools to answer these questions. We found that instability can occur when the resupply of a growth substrate (DOC) is (via a positive feedback loop) dependent on its abundance. We identified a conservative, sufficient condition on model parameters to ensure stability of EPs. Interactive effects of environmental conditions and parameters describing microbial physiology point to the relevance of basic ecological principles for avoidance of unrealistic (i.e. unstable) simulation outcomes. These insights can help to improve applicability of microbial-explicit models, aid our understanding of the dynamics of these models and highlight the relation between mathematical requirements and (*in silico*) microbial ecology.

1 Introduction

Current Earth system models (ESMs) have very simplified representations of soil organic carbon (SOC) dynamics (Bradford et al., 2016; Todd-Brown et al., 2013; Varney et al., 2022). Accuracy in matching observed SOC stocks and turnover times has not significantly improved in the latest ensemble of ESMs used in the Coupled Model Intercomparison Project (CMIP, CMIP 6) (Varney et al., 2022) – with uncertainty about SOC responses to climate change remaining high (Todd-Brown et al., 2013; Varney et al., 2022). Consequently, a need to improve and diversify description of SOC dynamics in ESMs has been identified (Bradford et al., 2016; Todd-Brown et al., 2013; Varney et al., 2022; Wieder et al., 2015, 2018). Current ESMs employ linear degradation kinetics to simulate SOC degradation (Todd-Brown et al., 2013), missing to integrate our current understanding of major controls on SOC fate and to acknowledge the uncertainties in describing these processes (Abs et al., 2023; Bradford et al.,



25 2016; Wieder et al., 2015, 2018). Non-linear, microbial-explicit SOC models can improve model-data agreement (Hararuk et al., 2015; Wieder et al., 2013). These models vary in number and identity of C pools and degree of non-linearity (e.g. Allison et al., 2010; Manzoni and Porporato, 2009; Schimel and Weintraub, 2003; Wang et al., 2013, 2015; Wieder et al., 2014, 2015). Among these models, the AWB (Allison-Wallenstein-Bradford) model (Allison et al., 2010) has emerged as an archetypal model structure to study the influence of soil microbial processes on carbon stocks (e.g. Abs et al., 2022; Calabrese et al., 30 2022; Georgiou et al., 2017; Hararuk et al., 2015; Tao et al., 2023; Wieder et al., 2015). The AWB model explicitly represents pools of microbial biomass, extracellular enzymes produced by microbes, polymeric SOC that is not available for microbial uptake, and a pool of available dissolved organic carbon (DOC) produced from enzymatic depolymerization of SOC (Allison et al., 2010, Fig. 1a). With only four C pools and commonly two non-linear terms, the AWB model retains a comparably simple structure and remains somewhat analytically tractable.

35 While better at predicting modern day SOC stocks, microbial-explicit SOC models are known to exhibit oscillatory behaviour (e.g. Georgiou et al., 2017; Manzoni and Porporato, 2007; Sierra and Müller, 2015; Wang et al., 2014, 2016). Such oscillations can represent carbon-microbe dynamics observed at small spatial scales (see e.g. discussion in Manzoni and Porporato, 2007) but are unfavourable for application at larger spatial and temporal scales, where such oscillations are generally not observed (Georgiou et al., 2017; Wang et al., 2014). A few studies have analysed the oscillatory properties of some microbial- 40 explicit SOC models (Georgiou et al., 2017; Manzoni and Porporato, 2007; Wang et al., 2014, 2016). These studies characterized the dynamics exhibited after a perturbation around a model's equilibrium (i.e., when all state variables are at steady state): does a model directly converge back to its previous equilibrium or does it approach the equilibrium with dampened oscillations? Different degrees of oscillatory behaviour have been described, but generally these models were found to be stable (that is, they do converge back to their previous equilibrium) for given parametrizations or if they follow basic principles such as mass 45 conservation and dependence of fluxes on source pools (Sierra and Müller, 2015; Wang et al., 2014, 2016). Stable oscillatory behaviour, however, is only one of the possible dynamics such non-linear models can exhibit. In fact, these models can also be unstable (that is after perturbation a model does not converge back to its previous equilibrium) (Abs et al., 2022; Raupach, 2007; Schimel and Weintraub, 2003; Sierra and Müller, 2015), but the occurrence of unstable equilibria in microbial-explicit SOC models remains largely unexplored. While unstable equilibrium points exist analytically, they can never be reached by 50 transient simulations. Thus, model parameterizations that yield unstable equilibria can lead to unpredictable simulation outcomes as amplifying oscillations can occur, expected equilibrium states are not reached (because they are unstable) hindering convergence in model spin-up, or (some) state variables might collapse (e.g. Fig. 1b, yellow line). Further, if C stocks are predicted based on analytical steady state solutions, unstable equilibria might lead to unrealistic predictions, mismatching outcomes from dynamic simulations. To increase reliability of model predictions and model applicability, it is important to 55 understand when and for what reasons microbial-explicit SOC models become unstable.

In this contribution, we study an archetypal microbial-explicit SOC model (based on the AWB model, Allison et al., 2010, and some simplified versions of it) to answer the questions: 1) What mechanisms in microbial-explicit SOC models (model structures, used kinetic formulations, and parameter values) cause unstable equilibrium points to emerge? and 2) how can we select model structures and/or constrain model parameters to ensure stability of equilibrium points?

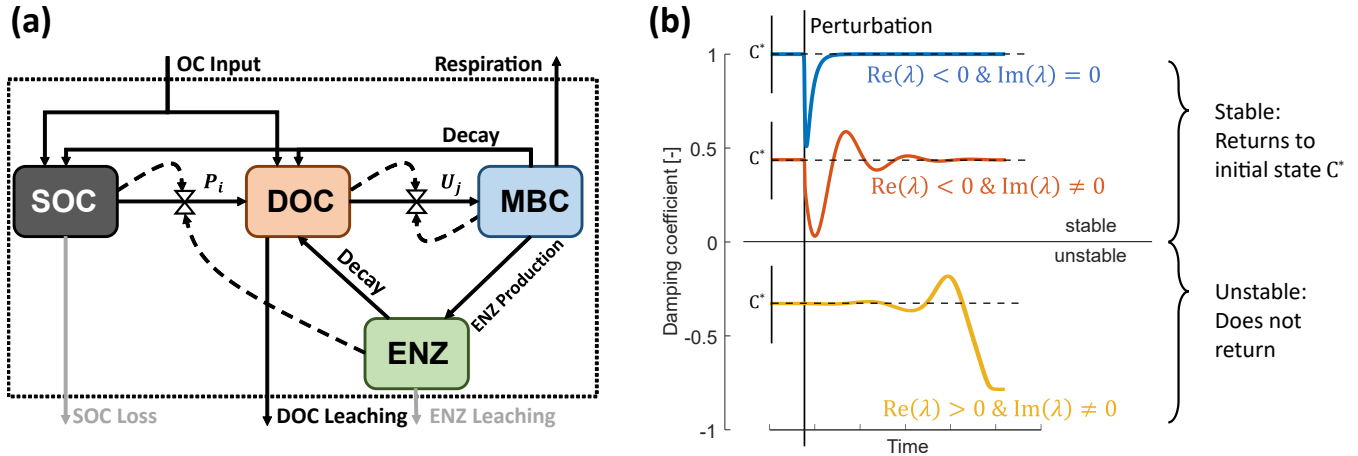


Figure 1. Model schematics of the archetypal microbial-explicit SOC model (a) and its relevant stability behaviours (b). Colored boxes in (a) indicate the state variables soil organic carbon (SOC), dissolved organic carbon (DOC) microbial biomass carbon (MBC), and extracellular enzymes (ENZ). Solid arrows indicate carbon fluxes and dashed arrows connected to valve symbols indicate controls over the non-linear kinetic. Grey arrows indicate processes neglected in some analyses. The dotted box delineates the system’s boundary. Colored lines in (b) illustrate the dynamics of a state variable relative to its steady state value (C^*) following a perturbation for a stable node (damping coefficient = 1; blue line), a stable focus ($0 < \text{damping coefficient} < 1$; red line), and an unstable focus ($-1 < \text{damping coefficient} < 0$; yellow line). The subplot axes are centered at the value of their respective damping coefficient.

60 2 Methods

2.1 Archetypal microbial-explicit SOC model

We start by defining the C mass balance equations for a system encompassing SOC (S), dissolved organic C (DOC, D), microbial biomass C (MBC, B), and extracellular enzyme C (ENZ, E) (eq. 1 - 4). The C compartments and flows are illustrated in Fig. 1a and symbols for the variables and fluxes are defined in Table 1 and 3. The C mass balance equations are written as a system of ordinary differential equations (ODE), where for convenience the fluxes are aligned vertically according to their meaning (from left to right: inputs, depolymerization, uptake and metabolism, decay, and finally abiotic losses)

$$\frac{dS}{dt} = f_I I - P + f_D r_B D_B - L_S \quad (1)$$

$$\frac{dD}{dt} = (1 - f_I) I + P - U + (1 - f_D) r_B D_B + D_E - L_D \quad (2)$$

$$\frac{dB}{dt} = y_B U - R_E - D_B \quad (3)$$

$$70 \quad \frac{dE}{dt} = (y_m - y_B) U + R_E - D_E - L_E \quad (4)$$



Organic matter enters the system with flux I that is partitioned between SOC and DOC depending on the fraction f_I . SOC is depolymerized by extracellular enzymes at rate P and transferred to the DOC pool. DOC is directly available for microbial uptake at rate U . Both P and U are non-linear functions that can take on various forms (Table 2).

Microbes assimilate the substrate with a maximal efficiency $y_m \leq 1$ that is limited by physiological and/or thermodynamic constraints (Chakrawal et al., 2022) and use the substrate either for growth (i.e. biomass production at rate $y_B U$) or to produce extracellular enzymes (at rate $(y_m - y_B)U$). We denote this uptake-dependent pathway of extracellular enzyme production as “inducible” ENZ production. An alternative or complementary mode of ENZ production is the biomass-dependent “constitutive” ENZ production at rate R_E given by

$$R_E = m_E B \quad , \quad (5)$$

where m_E is the rate constant of constitutive ENZ production. In both formulations, we assumed that respiratory costs associated with enzyme production are already included in the growth respiration (proportional to $1 - y_m$). Two limiting cases can be derived from this general description of extracellular enzyme production:

$$\text{Only constitutive ENZ production:} \quad y_B = y_m \quad (6)$$

$$\text{Only inducible ENZ production:} \quad m_E = 0 \quad . \quad (7)$$

Both MBC and ENZ are assumed to decay with a linear decay rate D_i

$$D_i = d_i i \quad , (i = B, E), \quad (8)$$

but we also consider density-dependent microbial decay as an alternative to the linear kinetic ($D'_B = d'_B B^b$ with $1 < b \leq 2$; Georgiou et al., 2017). All decayed ENZ are assumed to return to the DOC pool while only a fraction r_B of the decayed microbial biomass is recycled in the system and partitioned between SOC and DOC according to the factor f_D . In turn, $(1 - r_B)D_B$ represents linear microbial maintenance respiration. SOC, DOC and ENZ can have abiotic losses L_i (e.g. erosion, leaching, ...)

$$L_i = l_i i \quad , (i = S, D, E) \quad . \quad (9)$$

The system of eq. 1 - 4 constitutes a model of SOC cycling of varying complexity depending on the chosen kinetics. We use this system as a starting point for our analysis, but reduce it to simpler variants to derive specific analytical results (Sect. 2.2).

Commonly, depolymerization of SOC by extracellular enzymes is described by either multiplicative (m), forward Michaelis-Menten (f), reverse Michaelis-Menten (r) (Schimel and Weintraub, 2003) or equilibrium chemistry approximation (ECA, e) (Tang and Riley, 2013) kinetics. Table 2 lists the respective formulations of P_i ($i = m, f, r, e$), where v_i^p is the maximal depolymerization rate coefficient and K_i^p the respective half-saturation constant. The uptake of DOC by microbes can be described with similar formulations U_j ($j = m, f$), simply by replacing S for D and E for B (Table 2), where v_j^u is the maximal uptake rate coefficient and K_j^u the respective half-saturation constant.



Table 1. Description of all state variables and fluxes.

Symbol	Description	Unit
<i>State Variables</i>		
S	Soil organic carbon (SOC)	mg C g^{-1}
D	Dissolved organic carbon (DOC)	mg C g^{-1}
B	Microbial biomass (MBC)	mg C g^{-1}
E	Extracellular enzymes (ENZ)	mg C g^{-1}
<i>Fluxes</i>		
I	Organic carbon input	$\text{mg C g}^{-1} \text{ d}^{-1}$
P	Depolymerization of SOC	$\text{mg C g}^{-1} \text{ d}^{-1}$
U	Microbial uptake of DOC	$\text{mg C g}^{-1} \text{ d}^{-1}$
L_S	Loss of SOC	$\text{mg C g}^{-1} \text{ d}^{-1}$
L_D	Leaching of DOC	$\text{mg C g}^{-1} \text{ d}^{-1}$
L_E	Leaching of extracellular enzymes	$\text{mg C g}^{-1} \text{ d}^{-1}$
D_B	Decay of microbial biomass	$\text{mg C g}^{-1} \text{ d}^{-1}$
D_E	Decay of extracellular enzymes	$\text{mg C g}^{-1} \text{ d}^{-1}$
R_E	Constitutive production of extracellular enzymes	$\text{mg C g}^{-1} \text{ d}^{-1}$

Table 2. Employed non-linear kinetics for the depolymerization rate P_i and uptake rate U_j . m : multiplicative, f : forward Michaelis-Menten, r : reverse Michaelis-Menten (Schimel and Weintraub, 2003), e : equilibrium chemistry approximation (Tang and Riley, 2013). U_r and U_e are not used in our analysis.

Kinetic ($i j$)	P_i	U_j
m	$v_m^p SE$	$v_m^u DB$
f	$v_f^p \frac{S}{K_f^p + S} E$	$v_f^u \frac{D}{K_f^u + D} B$
r	$v_r^p S \frac{E}{K_r^p + E}$	–
e	$v_e^p \frac{SE}{K_e^p + S + E}$	–

Many combinations of depolymerization and uptake kinetics are possible. For model versions with both non-linear terms we limit our analysis to only a few combinations of depolymerization and uptake kinetics (indicated by the subscript $i \times j$ for the i -th depolymerization kinetic and j -th uptake kinetic), namely: $m \times m$, $f \times f$, and $r \times f$. The first combination employing only multiplicative kinetics facilitates analytical tractability; the second combination is commonly used in other models (e.g. Allison et al., 2010; Georgiou et al., 2017; Tao et al., 2023); the third combination is based on conclusions of Tang and Riley (2019) that $r \times f$ might be an appropriate (and analytically tractable) approximation of ECA kinetics (Table 4).

Here we define the Jacobian matrix of partial derivatives for the four-pool model, which is used in the stability analyses in later sections. To improve analytical tractability of the four-pool model we neglect abiotic losses of SOC and ENZ by setting



$L_S = L_E = 0$ and limit the analytical analysis only to the case of constitutive ENZ production ($y_B = y_m$, eq. 6) (Table 4).

110 With these simplification, the Jacobian matrix $J_{i \times j}^{SDBE}$ of the four-pool model is a 4×4 matrix given by

$$J_{i \times j}^{SDBE} = \begin{bmatrix} \frac{\partial \dot{S}}{\partial S} & \frac{\partial \dot{S}}{\partial D} & \frac{\partial \dot{S}}{\partial B} & \frac{\partial \dot{S}}{\partial E} \\ \frac{\partial \dot{D}}{\partial S} & \frac{\partial \dot{D}}{\partial D} & \frac{\partial \dot{D}}{\partial B} & \frac{\partial \dot{D}}{\partial E} \\ \frac{\partial \dot{B}}{\partial S} & \frac{\partial \dot{B}}{\partial D} & \frac{\partial \dot{B}}{\partial B} & \frac{\partial \dot{B}}{\partial E} \\ \frac{\partial \dot{E}}{\partial S} & \frac{\partial \dot{E}}{\partial D} & \frac{\partial \dot{E}}{\partial B} & \frac{\partial \dot{E}}{\partial E} \end{bmatrix} = \begin{bmatrix} -\frac{\partial P_i}{\partial S} & 0 & f_D r_B d_B & -\frac{\partial P_i}{\partial E} \\ \frac{\partial P_i}{\partial S} & -l_D - \frac{\partial U_j}{\partial D} & (1 - f_D) r_B d_B - \frac{\partial U_j}{\partial B} & d_E + \frac{\partial P_i}{\partial E} \\ 0 & y_m \frac{\partial U_j}{\partial D} & y_m \frac{\partial U_j}{\partial B} - (m_E + d_B) & 0 \\ 0 & 0 & m_E & -d_E \end{bmatrix} \quad (10)$$

where $\frac{\partial x}{\partial y}$ is the partial derivative of x with respect to y and \dot{x} is used to denote $\frac{dx}{dt}$ so that e.g. $\frac{\partial \dot{S}}{\partial S} = \frac{\partial}{\partial S} \left(\frac{dS}{dt} \right)$. Keeping general depolymerization and uptake kinetics P_i and U_j is useful as it allows to analyse $J_{i \times j}^{SDBE}$ irrespective of the specific kinetics.

2.2 Reduced models for analytical analysis

115 To identify which and how structural elements of the four-pool model with two non-linear kinetics affect model stability, we introduce two reduced model versions:

1. the *SBE* (SOC-MBC-ENZ) model, neglecting DOC dynamics, and
2. the *SDB* (SOC-DOC-MBC) model, assuming ENZ to be at quasi-steady state.

Both model versions have only three pools, but are different as in the *SBE* model only one non-linear term remains, while the
 120 *SDB* model still has both non-linear depolymerization and uptake kinetics. We analyze the former, less non-linear model for all depolymerization kinetics listed in Table 2 with both constitutive and inducible ENZ production pathways and including abiotic losses of S and E (Table 4). In contrast, we analyze the latter, more non-linear model, after applying the same simplifying assumptions as for the four-pool model (Table 4) – that is we set $L_S = L_E = 0$, $y_B = y_m$, and only consider three combinations of depolymerization and uptake kinetics ($m \times m$, $f \times f$, and $r \times f$).

125 2.2.1 *SBE* model

DOC dynamics are neglected in the *SBE* (SOC-MBC-ENZ) model. Instead it is assumed that any organic carbon that is made available by depolymerization of SOC is directly taken up by microbes – that is $U = P$. The flux of decayed extracellular enzymes D_E enters the SOC pool and the partitioning factors f_I and f_D are set to 1. The resulting system of equations is given for the i -th kinetic formulation for P (Table 2) by

$$130 \quad \frac{dS}{dt} = I - P_i + r_B D_B + D_E - L_S \quad (11)$$

$$\frac{dB}{dt} = y_B P_i - R_E - D_B \quad (12)$$

$$\frac{dE}{dt} = (y_m - y_B) P_i + R_E - D_E - L_E \quad (13)$$

Note that in this formulation, unless ENZ production is purely constitutive (eq. 6), ENZ production is (partly) independent of microbial biomass (as P_i only depends on E and not on B). Consequently, as soon as there are extracellular enzymes that
 135 catalyze depolymerization, further enzyme production entails.



For this model version, the Jacobian matrix J_i^{SBE} is given by

$$J_i^{SBE} = \begin{bmatrix} \frac{\partial \dot{S}}{\partial S} & \frac{\partial \dot{S}}{\partial B} & \frac{\partial \dot{S}}{\partial E} \\ \frac{\partial \dot{B}}{\partial S} & \frac{\partial \dot{B}}{\partial B} & \frac{\partial \dot{B}}{\partial E} \\ \frac{\partial \dot{E}}{\partial S} & \frac{\partial \dot{E}}{\partial B} & \frac{\partial \dot{E}}{\partial E} \end{bmatrix} = \begin{bmatrix} -l_s - \frac{\partial P_i}{\partial S} & r_B d_B & d_E - \frac{\partial P_i}{\partial E} \\ y_B \frac{\partial P_i}{\partial S} & -(d_B + m_E) & y_B \frac{\partial P_i}{\partial E} \\ (y_m - y_B) \frac{\partial P_i}{\partial S} & m_E & (y_m - y_B) \frac{\partial P_i}{\partial E} - (d_E + l_E) \end{bmatrix}. \quad (14)$$

2.2.2 SDB model

In the *SDB* (SOC-DOC-MBC) model, the extracellular enzyme pool is assumed to be at quasi-steady state, that is $\frac{dE}{dt} = 0$.

140 With $L_E = 0$ and $y_B = y_m$ we obtain the quasi-steady state concentration of E from eq. 4 as

$$E^{qss} = \frac{m_E}{d_E} B. \quad (15)$$

The *SDB* model is obtained by substituting E^{qss} for E in eq. 1 - 3, which with $L_S = 0$ yields

$$\frac{dS}{dt} = f_I I - P_i^{qss} + f_D r_B D_B \quad (16)$$

$$\frac{dD}{dt} = (1 - f_I) I + P_i^{qss} - U_j + (1 - f_D) r_B D_B + D_E^{qss} - L_D \quad (17)$$

$$145 \frac{dB}{dt} = y_m U_j - R_E - D_B. \quad (18)$$

In this model version, two non-linearities remain. Substituting E^{qss} for E in D_E and P_i we obtain $D_E^{qss} = R_E$ and $P_i^{qss} = f(S, B)$, respectively. The Jacobian matrix $J_{i \times j}^{SDB}$ of partial derivatives is given by

$$J_{i \times j}^{SDB} = \begin{bmatrix} \frac{\partial \dot{S}}{\partial S} & \frac{\partial \dot{S}}{\partial D} & \frac{\partial \dot{S}}{\partial B} \\ \frac{\partial \dot{D}}{\partial S} & \frac{\partial \dot{D}}{\partial D} & \frac{\partial \dot{D}}{\partial B} \\ \frac{\partial \dot{B}}{\partial S} & \frac{\partial \dot{B}}{\partial D} & \frac{\partial \dot{B}}{\partial B} \end{bmatrix} = \begin{bmatrix} -\frac{\partial P_i^{qss}}{\partial S} & 0 & -\frac{\partial P_i^{qss}}{\partial B} + f_D r_B d_B \\ \frac{\partial P_i^{qss}}{\partial S} & -\frac{\partial U_j}{\partial D} - l_D & \frac{\partial P_i^{qss}}{\partial B} - \frac{\partial U_j}{\partial B} + (1 - f_D) r_B d_B + m_E \\ 0 & y_m \frac{\partial U_j}{\partial D} & y_m \frac{\partial U_j}{\partial B} - m_E - d_B \end{bmatrix}. \quad (19)$$

2.3 Stability analysis

150 Stability behaviour here refers to how a model at equilibrium (that is all state variables C are at steady state [denoted as C^*] – i.e. their respective ODEs are equal to zero: $\frac{dC}{dt} = 0$) behaves after a small perturbation around this equilibrium. For non-linear systems, this behaviour is determined by the eigenvalues (λ) of the Jacobian matrix J evaluated at an equilibrium (denoted as $J|_*$; $\text{eig}(J|_*) = \lambda$) (e.g. Argyris et al., 2015). Briefly, if the real parts of *all* λ are negative ($\text{Re}(\lambda) < 0$) the equilibrium is stable: the system will converge back to this equilibrium after a perturbation. Instead, if *one or more* eigenvalues have positive real parts ($\text{Re}(\lambda) > 0$) the equilibrium is unstable and the system will not return to the same state. If the eigenvalues additionally have non-zero imaginary parts ($\text{Im}(\lambda) \neq 0$) oscillations around the equilibrium occur (Fig. 1b). Stability analysis is described in more details in e.g., Argyris et al. (2015).

2.3.1 Analytical approach

160 Because the eigenvalues of the Jacobian matrix can be analytically cumbersome even in the comparably compact three-pool models, we instead evaluate the Routh-Hurwitz criterion (e.g. Argyris et al., 2015; Horn and Johnson, 1991) for $J|_*$. The Routh-Hurwitz criterion states that all $\text{Re}(\lambda)$ have negative signs, if, and only if:



1. all coefficients a_i of the characteristic polynomial $\det(J|_* - \mathbf{1}\lambda) = 0$ (where $\mathbf{1}$ is the identity matrix; eq. 20 & 21) are positive (i.e. $a_i > 0$), and
2. $a_1 a_2 - a_3 > 0$ (if $J|_*$ is a 3×3 matrix) or $a_1 a_2 a_3 - a_3^2 - a_1^2 a_4 > 0$ (if $J|_*$ is a 4×4 matrix).

165 Thus, by applying the Routh-Hurwitz criterion we can analytically evaluate the stability around the equilibrium points of the non-linear systems given by the three- and four-pool models without directly evaluating λ analytically. The characteristic polynomial for a 3×3 matrix is given by

$$\lambda^3 + a_1 \lambda^2 + a_2 \lambda + a_3 = 0 \quad (20)$$

and for a 4×4 matrix is

$$170 \quad \lambda^4 + a_1 \lambda^3 + a_2 \lambda^2 + a_3 \lambda + a_4 = 0 \quad . \quad (21)$$

In both cases, a_1 is the negative trace of $J|_*$ ($a_1 = -\text{tr}(J|_*)$).

2.3.2 Numerical simulations

We also compute λ and the steady state values of the state variables numerically. If not otherwise specified, 100 000 Monte Carlo simulations were produced by randomly drawing parameter values from (log-)uniform distributions using a latin-
 175 hypercube sampling algorithm (MATLAB R2022b's `lhsdesign` function; The MathWorks Inc., 2022). All parameters and their respective ranges are listed in Table 3. Partitioning coefficients were sampled from uniform distributions while rate constants were \log_{10} -transformed before sampling.

Following Georgiou et al. (2017), the stability of equilibria was evaluated using the “damping coefficient” given by

$$\zeta = \min \left(\frac{-\text{Re}(\lambda)}{\sqrt{\text{Re}(\lambda)^2 + \text{Im}(\lambda)^2}} \right) \quad , \quad (22)$$

180 which ranges between -1 and 1. ζ has positive values only if all $\text{Re}(\lambda) < 0$ indicating a stable equilibrium and negative values if any $\text{Re}(\lambda) > 0$ indicating an unstable equilibrium. For $\text{Im}(\lambda) = 0$, ζ is either 1 or -1 indicating no oscillations, while $-1 < \zeta < 1$ for $\text{Im}(\lambda) \neq 0$ indicates that oscillations occur.

Numerical simulations were carried out in MATLAB 2022b (The MathWorks Inc., 2022).

2.3.3 Classification of equilibrium points

185 Our analyses only consider physically meaningful equilibrium points - that is, only equilibrium points for which all state variables are simultaneously positive and real. Within the physically meaningful equilibrium points we distinguish three categories:

1. stable: all physically meaningful equilibrium points that are stable (i.e., stable node or focus points, Argyris et al., 2015),
2. stable and plausible: all physically meaningful equilibrium points that are stable and also give plausible numerical results



Table 3. Description of all parameters, their units, and used ranges for Monte Carlo simulations. Where applicable, parametrizations of limiting cases are separated by |. Parameter ranges where derived from Hararuk et al. (2015); Tao et al. (2023) and Cotrufo and Lavelle (2022). Baseline values were based on “conventional” values defined by Tao et al. (2023). See Supplemental Information (SI) Sect. 1 for derivation of parameter ranges for m , r , and l kinetics as well as for d'_B and I .

Symbol	Description	Unit	Baseline	Range
<i>Rate Constants</i>				
I	Organic C input rate	mg C g ⁻¹ d ⁻¹	varied	$1.88 \cdot 10^{-4} - 2.43 \cdot 10^{-2}$
v_m^p	Depolymerization rate coefficient (m)	g mg C ⁻¹ d ⁻¹	$1.99 \cdot 10^{-1}$	$9.13 \cdot 10^{-3} - 5.48 \cdot 10^3$
v_f^p	Depolymerization rate coefficient (f)	d ⁻¹	$5.93 \cdot 10^1$	$9.13 - 2.74 \cdot 10^5$
v_r^p	Depolymerization rate coefficient (r)	d ⁻¹	$2.49 \cdot 10^{-1}$	$9.13 \cdot 10^{-2} - 2.74$
K_f^p	Depolymerization half-saturation constant (f)	mg C g ⁻¹	$3.00 \cdot 10^2$	$5.00 \cdot 10^1 - 1.00 \cdot 10^3$
K_r^p	Depolymerization half-saturation constant (r)	mg C g ⁻¹	$2.00 \cdot 10^{-1}$	$2.50 \cdot 10^{-2} - 3.00$
v_m^u	Uptake rate coefficient (m)	g mg C ⁻¹ d ⁻¹	1.25	$3.04 \cdot 10^{-2} - 1.10 \cdot 10^2$
v_f^u	Uptake rate coefficient (f)	d ⁻¹	$2.49 \cdot 10^{-1}$	$9.13 \cdot 10^{-2} - 2.74$
v_l^u	Linear uptake rate coefficient	d ⁻¹	1.25	$3.04 \cdot 10^{-3} - 1.10 \cdot 10^1$
K_f^u	Uptake half-saturation constant (f)	mg C g ⁻¹	$2.00 \cdot 10^{-1}$	$2.50 \cdot 10^{-2} - 3.00$
l_S	Loss rate coefficient of SOC	d ⁻¹	0	–
l_D	Leaching rate coefficient of DOC	d ⁻¹	varied 0	$2.74 \cdot 10^{-4} - 2.74 \cdot 10^{-1} 0$
l_E	Leaching rate coefficient of extracellular enzymes	d ⁻¹	0	–
d_B	Decay rate coefficient of biomass	d ⁻¹	$4.81 \cdot 10^{-3}$	$1.37 \cdot 10^{-3} - 2.74 \cdot 10^{-1}$
d'_B	Density-dependent d_B	g mg C ⁻¹ d ⁻¹	–	$1.37 \cdot 10^{-2} - 2.74$
d_E	Decay rate coefficient of extracellular enzymes	d ⁻¹	$2.49 \cdot 10^{-2}$	$2.74 \cdot 10^{-3} - 2.74$
m_E	Constitutive enzyme production rate coefficient	d ⁻¹	$1.25 \cdot 10^{-4}$	$8.22 \cdot 10^{-5} - 1.83 \cdot 10^{-4} 0$
<i>Partitioning Coefficients</i>				
r_B	Recycling efficiency of decayed biomass	1	1.00	0.20 – 1.00
y_m	Maximal yield	1	0.60	0.01 – 0.80
y_B	Fraction of uptake going to biomass production	1	y_m	$0 < y_B \leq y_m y_m$
f_I	Fraction of input going to SOC	1	0.90	0.50 – 1.00
f_D	Fraction of decayed biomass going to SOC	1	0.50	0.50 – 1.00



190 3. unstable: all physically meaningful equilibrium points that are not stable (i.e., unstable node or focus points, Argyris et al., 2015).

Based on data synthesized by Wang et al. (2013) and educated guesses we applied the following conditions for considering results as “plausible”: $tOC = SOC + DOC + MBC + ENZ \leq 500 \text{ mgC g}^{-1}$ (=50%), $DOC/tOC < 0.01$, $MBC/tOC < 0.05$, and $ENZ/MBC < 0.1$, where tOC indicates the total organic carbon content (the sum of all four carbon pools).

2.3.4 Causal loop analysis

195 Additionally to the mathematical analysis of equilibrium points and their stability, we present causal loop diagrams that qualitatively summarize causal links in a system and the feedbacks they create (Haraldsson, 2004). This analysis can help to understand the behaviour a system exhibits after a perturbation around an equilibrium point. In a causal loop diagram, causal connections are depicted by arrows, tying a cause (at the tail of the arrow) to its direct effect (at the head of the arrow) (Haraldsson, 2004). The sign of the causal relation (+ or −) depends on whether an isolated change in one element causes another to change in the same (+) or opposite (−) direction of the initial change (relative to the unchanged state) (Haraldsson, 2004; Richardson, 1986). For example, a decrease in the microbial uptake rate would lead to relatively less microbial biomass (compared to the case that the uptake rate had not changed), describing a positive causal relation. Closed loops with zero or an even number of negative interactions are denoted as positive or reinforcing feedback loops R , and closed loops with a odd number of negative interactions as a negative or balancing feedback loops B (Haraldsson, 2004; Richardson, 1986).

205 3 Results

Table 4. Summary of analysed models, respective simplifying assumptions, and type of analysis (ana. = analytical, num. = numerical).

Model	# Pools	Kinetics	Simplifying Assumptions	Analysis
SBE	3	m, f, r, e	none	ana.
SDB	3	$m \times m, f \times f, r \times f$	$L_S = L_E = 0;$	$y_B = y_m$ ana.
$SDBE$	4	$m \times m, f \times f, r \times f$	$L_S = L_E = 0;$	$\begin{cases} y_B = y_m & \text{ana. + num.} \\ m_E = 0 & \text{num.} \end{cases}$

We analyzed three model versions with slightly different model structures (number of state variables and/or non-linearities; Table 4, Sect. 2.2). We first present analytical results on the simpler three-pool models with one (SBE) and two non-linear terms (SDB), followed by analytical and numerical results on the four-pool $SDBE$ model (Table 4). We use causal loop diagrams to qualitatively interpret these results.



210 3.1 *SBE* model: neglecting DOC dynamics

3.1.1 Steady state solutions

Table 5. Summary of steady state solutions of the three-pool *SBE* model for different kinetics of depolymerization. The “biotic” equilibrium solutions for microbial biomass and extracellular enzymes have the same form for any chosen kinetic.

	Kinetic (i)	$S_{k,i}^*$	$B_{k,i}^*$	$E_{k,i}^*$
abiotic ($k = 0$)	i	$\frac{I}{l_S}$	0	0
biotic ($k = 1$)	m	$\frac{\alpha\beta}{v_m^p \eta}$		
	f	$\frac{\alpha\beta}{v_f^p \eta} \frac{K_f^p}{1 - \frac{\alpha\beta}{v_f^p \eta}}$	$\frac{\alpha y_B}{\omega} l_S (S_0^* - S_{1,i}^*)$	$\frac{\eta}{\alpha y_B} B_{1,i}^*$
	r	$\frac{\alpha\beta}{v_r^p \eta} \frac{K_r^p \omega + I \eta}{\omega + l_S \frac{\alpha\beta}{v_r^p}}$		
	e	$\frac{\alpha\beta}{v_e^p \eta} \frac{K_e^p \omega + I \eta}{\omega - \omega \frac{\alpha\beta}{v_e^p \eta} + l_S \frac{\alpha\beta}{v_e^p}}$		

For all kinetic descriptions of the depolymerization rate (Table 2), the three-pool *SBE* model has two equilibrium points (EPs). Of these, one is an “abiotic” equilibrium Q_0 , where only SOC exists and microbial biomass and extracellular enzymes are zero, i.e. $Q_0 = (S_0^*, 0, 0)$. Here the asterisk indicates a state variable at steady state and the subscript 0 signifies the “abiotic” solution. In turn, for each kinetic there exists an alternative “biotic” equilibrium point with non-zero microbial biomass and extracellular enzymes, $Q_{1,i} = (S_{1,i}^*, B_{1,i}^*, E_{1,i}^*)$. The steady state solutions for these equilibria depend on the i -th formulation used to describe P_i . All solutions are reported in Table 5, where for convenience parameters have been grouped as follows:

$$\alpha = d_E + l_E \quad (23)$$

$$\beta = d_B + m_E \quad (24)$$

$$220 \quad \eta = \underbrace{(y_m - y_B)}_{\geq 0} d_B + y_m m_E \quad (25)$$

$$\omega = \alpha\beta - \alpha y_B r_B d_B - \eta d_E \quad (26)$$

With these definitions and recalling that $0 < y_B \leq y_m < 1$ and $0 < r_B \leq 1$, we find that ω is always larger than zero. While the “abiotic” equilibrium is always positive, the “biotic” one is positive (and thus physically meaningful) only if

$$S_{1,i}^* < S_0^* \quad \rightarrow \quad l_S S_{1,i}^* < I, \quad (27)$$

225 i.e. if the linear SOC loss rate is smaller than SOC inputs. Note that for f and e kinetics it is additionally required that $\frac{\alpha\beta}{v_i^p \eta} < 1$ ($i = f, e$).

If abiotic loss of SOC and are neglected (i.e. $l_S = 0$), the “abiotic” equilibrium does not exist (SOC would accumulate at the constant rate I) and by eq. 27 the “biotic” equilibrium is always physically meaningful.



3.1.2 Stability analysis

230 To analyze whether a physically meaningful equilibrium point is also stable we apply the Routh-Hurwitz criterion to the Jacobian matrix J_i^{SBE} (eq. 14) evaluated at the k -th equilibrium point ($J_i^{SBE}|_{*,k}$) – either the “abiotic” ($k = 0$) or the “biotic” equilibrium ($k = 1$).

“Abiotic” equilibrium

First, we evaluate the parameter space in which the “abiotic” equilibrium is stable. Substituting the steady state solutions for Q_0 given in Table 5 into J_i^{SBE} (eq. 14) yields

$$J_i^{SBE}|_{*,0} = \begin{bmatrix} -l_s & r_B d_B & d_E - \frac{\partial P_i}{\partial E}|_{*,0} \\ 0 & -\beta & y_B \frac{\partial P_i}{\partial E}|_{*,0} \\ 0 & m_E & (y_m - y_B) \frac{\partial P_i}{\partial E}|_{*,0} - \alpha \end{bmatrix} . \quad (28)$$

For Q_0 to be stable by the Routh-Hurwitz criterion, it is required that all the coefficients a_i of the characteristic polynomial of $J_i^{SBE}|_{*,0}$ and additionally $a_1 a_2 - a_3$ be positive. By this we find that stability of Q_0 is conditional on the sufficient and necessary condition (SI Sect. 2.1)

$$240 \quad \frac{\partial P_i}{\partial E}|_{*,0} < \frac{\alpha \beta}{\eta} . \quad (29)$$

“Biotic” equilibrium

Next, we analyze the stability of the “biotic” equilibrium, by evaluating the Jacobian matrix J_i^{SBE} (eq. 14) around its “biotic” steady states $Q_{1,i}$ (Table 5)

$$J_i^{SBE}|_{*,1} = \begin{bmatrix} -l_s - \frac{\partial P_i}{\partial S}|_{*,1} & r_B d_B & d_E - \frac{\partial P_i}{\partial E}|_{*,1} \\ y_B \frac{\partial P_i}{\partial S}|_{*,1} & -\beta & y_B \frac{\partial P_i}{\partial E}|_{*,1} \\ (y_m - y_B) \frac{\partial P_i}{\partial S}|_{*,1} & m_E & (y_m - y_B) \frac{\partial P_i}{\partial E}|_{*,1} - \alpha \end{bmatrix} . \quad (30)$$

245 To evaluate the Routh-Hurwitz criterion it is convenient to re-express P_i in terms of $\frac{\partial P_i}{\partial E}$ as

$$P_i = \frac{\partial P_i}{\partial E} x_i^{-1} E , \quad (31)$$

where the factor x_i is introduced to maintain generality of this substitution for any P_i as defined in Table 2:

$$x_i = \begin{cases} 1 & \text{if } (i = m, f) \\ 1 - \frac{E}{K_r^p + E} & \text{if } i = r \\ 1 - \frac{E}{K_e^p + S + E} & \text{if } i = e \end{cases} . \quad (32)$$

Moreover, x_i has the convenient property $0 < x_i \leq 1$. The ensuing derivations hold for all x_i as long as $0 < x_i \leq 1$ and also
 250 for other kinetics P_j not explored here for which a $0 < x_j \leq 1$ can be found that satisfies eq. 31.



Substituting eq. 31 and $B_{1,i}^* = \frac{\alpha y_B}{\eta} E_{1,i}^*$ (Table 5) into eq. 13 evaluated at steady state yields

$$\frac{dE_i}{dt} = (y_m - y_B) \frac{\partial P_i}{\partial E} \Big|_{*,1} x_i^{-1} \Big|_{*,1} E_{1,i}^* + m_E \frac{\alpha y_B}{\eta} E_{1,i}^* - d_E E_{1,i}^* - l_E E_{1,i}^* = 0 \quad , \quad (33)$$

from which, for $E_{1,i}^* \neq 0$ we find

$$\frac{\partial P_i}{\partial E} \Big|_{*,1} = \alpha x_i \Big|_{*,1} \frac{1 - \frac{m_E y_B}{\eta}}{y_m - y_B} = \frac{\alpha \beta}{\eta} x_i \Big|_{*,1} \quad . \quad (34)$$

255 With this definition we obtain

$$J_i^{SBE} \Big|_{*,1} = \begin{bmatrix} -l_s - \frac{\partial P_i}{\partial S} \Big|_{*,1} & r_B d_B & d_E - \frac{\alpha \beta}{\eta} x_i \Big|_{*,1} \\ y_B \frac{\partial P_i}{\partial S} \Big|_{*,1} & -\beta & y_B \frac{\alpha \beta}{\eta} x_i \Big|_{*,1} \\ (y_m - y_B) \frac{\partial P_i}{\partial S} \Big|_{*,1} & m_E & \alpha \left(x_i \Big|_{*,1} - \frac{m_E y_B}{\eta} x_i \Big|_{*,1} - 1 \right) \end{bmatrix} \quad . \quad (35)$$

From this it can be seen that the trace of $J_i^{SBE} \Big|_{*,1}$ (the sum of the diagonal entries) is always negative, since $\frac{\partial P_i}{\partial S} \Big|_{*,1} > 0$ and $x_i \Big|_{*,1} \leq 1$; and thus $a_1 > 0$. Likewise it can be shown that all remaining coefficients of the characteristic polynomial are always positive and that $a_1 a_2 - a_3 > 0$ (see detailed analytical derivations in SI Sect. 2.1). Thus, all physically meaningful “biotic” equilibrium points of the three-pool *SBE* model are stable.

Fig. 2a shows a simplified causal loop diagram of the *SBE* model (sparing all loss and decay terms) that can help to understand the dynamic behaviour of the model after a perturbation around an equilibrium. The reinforcing loop R_1 describes the increase in microbial biomass with increasing depolymerization rate (\propto uptake rate), leading to increased ENZ production rate, ENZ concentration, and consequently a further increasing depolymerization rate. This reinforcing effect is dampened by the balancing loops B_1 (the depletion of SOC by depolymerization) and B_2 (the carbon cost of ENZ production). The reinforcing loop R_2 exists only if inducible ENZ production is considered ($y_B < y_m$; higher depolymerization stipulates the production of more extracellular enzymes, which promote depolymerization). R_1 and R_2 are not independent of each other and have to obey mass balance — i.e. per unit of uptake an increase in inducible ENZ production ($\propto y_m - y_B$) can only be achieved by reducing the built-up of microbial biomass (lowering y_B). An extreme case of this is $y_B = 0$; in this case, no microbial biomass is produced and only B_1 and R_2 remain. From the stability analysis, we obtained no condition on stability of physically meaningful equilibrium points in the *SBE* model. Thus, for any proportion of constitutive vs. inducible ENZ production, all physically meaningful “biotic” equilibria are also stable. That is, the dynamic behaviour of the model after a perturbation around its equilibrium is dominated by the balancing feedbacks, ensuring a convergence back to the equilibrium.

Exclusive stability of either “abiotic” or “biotic” equilibrium

275 We recall that for the “biotic” equilibrium to be physically meaningful it is required that $S_{1,i}^* < S_0^*$ (eq. 27); whereas for the “abiotic” equilibrium to be stable it is required by eq. 29 that $\frac{\partial P_i}{\partial E} \Big|_{*,0} < \frac{\alpha \beta}{\eta}$. This condition translates, e.g. for multiplicative kinetics to:

$$\frac{\partial P_m}{\partial E} \Big|_{*,0} = v_m^p S_0^* < \frac{\alpha \beta}{\eta} \quad \rightarrow \quad S_0^* < \frac{\alpha \beta}{v_m^p \eta} = S_{1,m}^* \quad . \quad (36)$$



This means that when the “biotic” equilibrium is physically meaningful the “abiotic” equilibrium is unstable and vice versa. Therefore, no region in the parameter space yields a physically meaningful bi-stability in which “biotic” and “abiotic” equilibria are simultaneously physically meaningful and stable. This holds for all evaluated kinetics (see SI Sect. 2.1 for the remaining analytical derivations).

3.2 SDB model: neglecting ENZ dynamics

3.2.1 Steady state solutions

Table 6. Summary of steady states for the three-pool *SDB* and four-pool *SDBE* model for different kinetics of depolymerization and uptake. The “abiotic” steady state is only defined for $l_S > 0$. “Biotic” steady states are given for $l_E = l_S = 0$ and $y_B = y_m$. $E_{k,i \times j}^\dagger$ signifies $E_{k,i \times j}^{qss}$ or $E_{k,i \times j}^*$ in the *SDB* respectively *SDBE* model. The “biotic” equilibrium solutions for microbial biomass and enzymes have the same form for any chosen kinetics.

	Kinetics	$S_{k,i \times j}^*$	$D_{k,i \times j}^*$	$B_{k,i \times j}^*$	$E_{k,i \times j}^\dagger$
abiotic ($k = 0$)	$i \times j$	$f_I \frac{I}{l_S}$	$(1 - f_I) \frac{I}{l_D}$	0	0
biotic ($k = 1$)	$m \times m$	$\frac{d_E}{y_m v_m^p m_E} \gamma_{m \times m}$	$\frac{\beta}{y_m v_m^u}$		
	$f \times f$	$\frac{d_E}{y_m v_f^p m_E} \gamma_{f \times f} \frac{K_f^p}{1 - \frac{d_E}{y_m v_f^p m_E} \gamma_{f \times f}}$	$K_f^u \frac{\beta}{y_m v_f^u - \beta}$	$\frac{y_m}{\pi} (I - l_D D_{1,i \times j}^*)$	$\frac{m_E}{d_E} B_{1,i \times j}^*$
	$r \times f$	$\frac{d_E}{y_m v_r^p m_E} \gamma_{r \times f} (K_r^p + E_{1,r \times f}^\dagger)$	$K_f^u \frac{\beta}{y_m v_f^u - \beta}$		

Table 6 reports the steady state solution of the three-pool *SDB* model, where for convenience parameters were grouped in

$$\gamma_{i \times j} = f_D r_B d_B y_m + \pi f_I \frac{I}{I - l_D D_{1,i \times j}^*} \quad (37)$$

and

$$\pi = \frac{1}{d_E} \omega(l_E = 0, y_B = y_m) = \underbrace{(1 - y_m) m_E}_{>0} + \underbrace{(1 - y_m r_B) d_B}_{>0} > 0 \quad (38)$$

Because an “abiotic” equilibrium exists only for $l_S > 0$ (Table 6) we only evaluate the stability of the “biotic” equilibrium and drop “1” from the subscript for conciseness. “Biotic” steady states are only physically meaningful for $I > l_D D_{i \times j}^*$ – meaning the DOC leaching flux can not be larger then the total OC input flux. With $f \times f$ and $r \times f$ kinetics it is additionally required that $\beta < y_m v_f^u$, implying that the maximal per-biomass assimilation rate $y_m v_f^u$ must be larger than the sum of all linear per-biomass loss terms $\beta = m_E + d_B$. For $f \times f$ kinetics it is additionally required that $\frac{d_E}{y_m v_f^p m_E} \gamma_{f \times f} < 1$ for steady states to be positive.

In absence of DOC leaching (for $l_D = 0$), with $m \times m$ and $f \times f$ kinetics $S_{i \times j}^*$ becomes independent of I while $B_{i \times j}^*$ and $E_{i \times j}^*$ are linear functions of I . In contrast, for $l_D = 0$, $S_{r \times f}^*$ is linearly dependent on OC input I . For $l_D > 0$, $S_{m \times m}^*$ is a function of $\frac{I}{I - l_D D_{m \times m}^*}$ causing $S_{m \times m}^*$ to decline with increasing inputs as $\frac{I}{I - l_D D_{m \times m}^*} \rightarrow 1$ for $I \gg l_D D_{m \times m}^*$. Only in $S_{r \times f}^*$ does I still appear in a linear term also for $l_D > 0$.



3.2.2 Stability analysis

300 The Jacobian matrix around the “biotic” equilibrium $J_{i \times j}^{SDB}|_*$ is given by eq. 19. Evaluating the coefficients of the characteristic polynomial and the requirement that $a_1 a_2 - a_3 > 0$ (SI Sect. 2.2) gives the necessary condition

$$a_1 a_2 - a_3 = X_{i \times j} + Y_{i \times j} > 0 \quad (39)$$

with

$$X_{i \times j} = \frac{\partial U_j}{\partial D} \Big|_* \left\{ \left(\frac{\partial U_j}{\partial D} \Big|_* + \frac{\partial P_i^{qss}}{\partial S} \Big|_* \right) \left(\frac{\partial P_i^{qss}}{\partial S} \Big|_* + y_m f_D r_B d_B - y_m \frac{\partial P_i^{qss}}{\partial B} \Big|_* \right) + \pi \frac{\partial U_j}{\partial D} \Big|_* \right\} \quad (40)$$

305 and

$$Y_{i \times j} = - \frac{\partial \dot{B}}{\partial B} \Big|_{*,j} \left\{ \frac{\partial P_i^{qss}}{\partial S} \Big|_* \left(\frac{\partial P_i^{qss}}{\partial S} \Big|_* - \frac{\partial \dot{B}}{\partial B} \Big|_{*,j} \right) + \frac{\partial U_j}{\partial D} \Big|_* \left(2 \cdot \frac{\partial P_i^{qss}}{\partial S} \Big|_* + y_m f_D r_B d_B - y_m \frac{\partial P_i^{qss}}{\partial B} \Big|_* + \pi \right) \right\} \quad (41)$$

both shown for $l_D = 0$ for conciseness (see full expressions with $l_D > 0$ in SI Sect. 2.2). The appearance of such a conditional statement means that in contrast to the *SBE* model, the *SDB* model can have physically meaningful but unstable EPs (i.e. if eq. 39-41 do not hold). A perturbation around such an unstable EP will cause the system to diverge from the EP. In this case, 310 the biotic pools (MBC and quasi-steady state ENZ) will collapse, while DOC will reach a steady state as $D_{0,i \times j}^*$ (for $l_D > 0$), and SOC will accumulate indefinitely.

$\frac{\partial \dot{B}}{\partial B} \Big|_{*,j}$ in eq. 41 is the lower right entry of $J_{i \times j}^{SDB}|_*$ (eq. 19) and is given by

$$\frac{\partial \dot{B}}{\partial B} \Big|_{*,j} = \frac{\partial}{\partial B} \frac{dB}{dt} \Big|_{*,j} = y_m \frac{\partial U_j}{\partial B} \Big|_* - m_E - d_B \quad (42)$$

For any choice of U_j that is linear in B (as is the case for U_m and U_f – compare Table 2) we find from solving $\frac{dB}{dt}$ (eq. 18) 315 at steady state that $y_m \frac{\partial U_{(m,f)}}{\partial B} \Big|_* = m_E + d_B$ and thus $\frac{\partial \dot{B}}{\partial B} \Big|_{*,(m,f)} = 0$, so that $Y_{i \times (m,f)} = 0$ (eq. 41). The only necessary and sufficient condition for stability of the *SDB* model in these cases is thus $X_{i \times j} > 0$ (eq. 40) (for $l_D = 0$, see SI Sect. 2.2 for the corresponding necessary condition for $l_D > 0$). However, the expression given by $X_{i \times j}$ does not allow for easy interpretation or application. We thus propose a sufficient (i.e. a more conservative or strict) condition for stability that is easier to trace analytically as

$$320 \frac{\partial P_i^{qss}}{\partial S} \Big|_* + y_m f_D r_B d_B \geq y_m \frac{\partial P_i^{qss}}{\partial B} \Big|_* \quad (43)$$

This sufficient condition for stability of “biotic” equilibrium points of the *SDB* model further holds for any $l_D \geq 0$ and thus in all cases relevant to our analysis (SI Sect. 2.2).

Described in words, this condition requires the depolymerization rate to be less sensitive to a change in microbial biomass than to a proportional change in SOC. Fig. 2b illustrates this relation in a simplified causal loop diagram. The reinforcing loop 325 R_1 causes the depolymerization rate (P_i^{qss}) to increase as the (quasi-steady state) ENZ concentration increases (quantified by $\frac{\partial P_i^{qss}}{\partial B} \Big|_*$). This then increases DOC concentration, uptake, and ultimately causes a further increase in microbial biomass and



(quasi-steady state) ENZ. This positive feedback is accelerated by an additional reinforcing feedback loop (R_2) that causes uptake to further increase as microbial biomass increases. The balancing loops B_2 and B_3 respectively describe the depletion of DOC with increasing uptake and the reduction of biomass as more extracellular enzymes are being produced. Lastly, the balancing loop B_1 causes SOC to change in the opposite direction than the depolymerization rate (i.e., SOC is depleted as depolymerization increases and relatively more SOC remains as depolymerization decreases), counteracting the initial change in P_i^{qss} (quantified by $\left. \frac{\partial P_i^{qss}}{\partial S} \right|_*$). Therefore, the sufficient stability condition in eq. 43 can be interpreted in the sense that the negative feedback B_1 must be quantitatively stronger than the positive feedback R_1 (by some factor y_m and buffered by a constant term; eq. 43).

In essence, the positive feedback R_1 can drive the system to overshoot or collapse: e.g., if microbial biomass or (quasi-steady state) ENZ concentration happens to decrease due to a perturbation, this will reduce the depolymerization rate, and following the positive feedback, result in further reduced MBC and (quasi-steady state) ENZ concentration. The biotic pools would collapse and the system would not be able to recover to its initial equilibrium (i.e. be unstable). Only if the entailing accumulation of SOC increases the depolymerization rate more than it is reduced by the depletion of (quasi-steady state) ENZ, will the system be able to recover and retain the biotic components (i.e. be stable). Beyond this sufficient condition for stability, the additional positive term $\pi \left. \frac{\partial U_j}{\partial D} \right|_*$ in $X_{i \times j}$ (eq. 40) might indicate the stabilizing influence of the balancing loop B_2 (Fig. 2b) and the recycling of ENZ and MBC to SOC (compare eq. 38).

We note that for linear uptake kinetics U_l , that is

$$U_l = v_l^u D \quad , \quad (44)$$

$Y_{i \times l}$ (eq. 41) does not vanish from eq. 39 since $\left. \frac{\partial U_l}{\partial B} \right|_* = 0$ and consequently from eq. 42

$$-\left. \frac{\partial \dot{B}}{\partial B} \right|_{*,l} = m_E + d_B > 0 \quad . \quad (45)$$

Because of its additional positive components, $Y_{i \times j}$ can be positive even if the sufficient condition of eq. 43 is not fulfilled. Thus, using U_l can help to ensure positivity of the all coefficients of the characteristic polynomial and $a_1 a_2 - a_3 > 0$. In the causal loop diagram linear uptake kinetics remove the positive feedback between uptake rate and biomass (R_2 in Fig. 2b vanishes). Although we could not show this analytically from eq. 39-41 & 45, numerical evaluation showed that for the chosen parameter spaces (Table 3) with linear uptake kinetics U_l physically meaningful EPs of the SDB model were always stable (SI Fig. S3c-d).

3.3 $SDBE$ model: full archetypal model

The four-pool $SDBE$ model with $L_S = L_E = 0$ and $y_B = y_m$ has the same steady state solutions as the three-pool SDB model, but now the solution for the ENZ pool is denoted as $E_{i \times j}^*$ because ENZ is not considered to be at quasi-steady state as in the SDB model (Table 6).

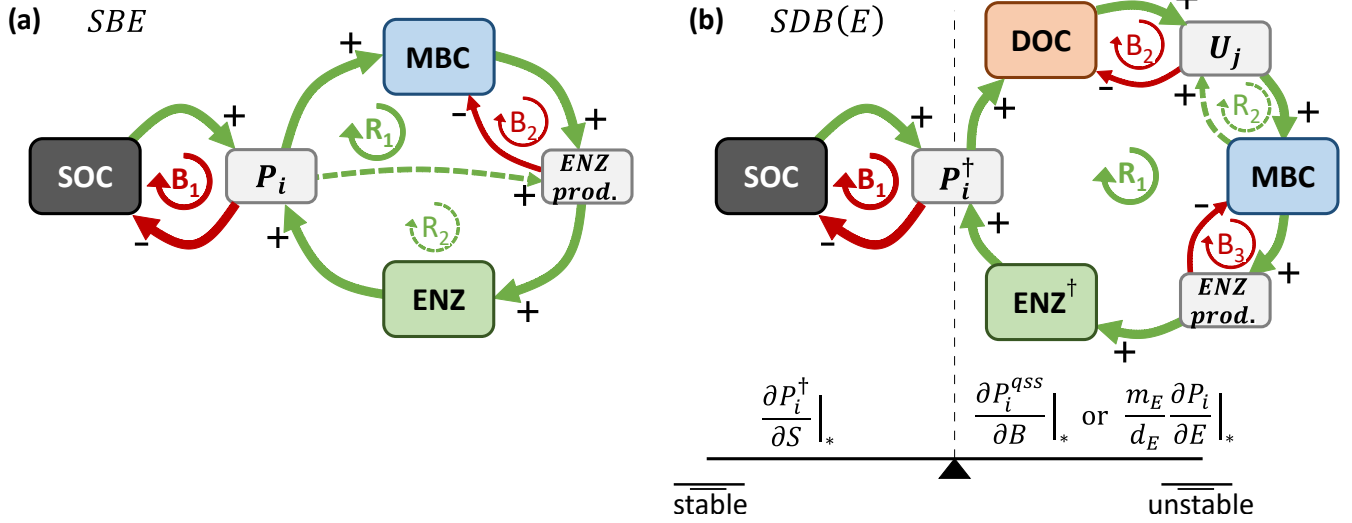


Figure 2. Simplified causal loop diagrams of the three-pool *SBE* (a) and four-pool *SDB* and *SDBE* models (b). Green arrows marked with “+” indicate positive and red arrows marked with “-” negative interactions. *R* signifies reinforcing and *B* balancing loops. In (a), the dashed green line (at *R*₂) indicates the effect of inducible ENZ production and vanishes if only constitutive ENZ production is considered. In (b), the dashed green line (at *R*₂) indicates the effect of biomass-dependent non-linear uptake kinetics and vanishes for biomass-independent uptake kinetics. In the *SDB* (*SDBE*) model P_i^\dagger and ENZ^\dagger signify P_i^{qss} (P_i) and $E_{i \times j}^{qss}$ ($E_{i \times j}^*$). The seesaw in (b) illustrates the balance between the partial derivatives in eq. 43 & 46 and how it affects stability.

3.3.1 Analytical stability analysis

In the four-pool *SDBE* model, the coefficients of the characteristic polynomial of $J_{i \times j}^{SDBE}$ (eq. 10) remain analytically tractable (SI Sect. 2.3). The trace of $J_{i \times j}^{SDBE}$ is always negative (and thus $-\text{tr}(J_{i \times j}^{SDBE}) = a_1 > 0$) and its determinant is always positive ($\det(J_{i \times j}^{SDBE}) = a_4 > 0$). However, the additional Routh-Hurwitz criterion for the 4×4 matrix $J_{i \times j}^{SDBE}$ (given by $a_1 a_2 a_3 - a_3^2 - a_1^2 a_4 > 0$) becomes analytically intractable. Despite this additional complexity, we can still draw some conclusions based on similarities between the *SDB* and *SDBE* models. Considering that in the *SDBE* model ENZ dynamics are explicitly represented (and thus e.g. $\frac{\partial P_i^{qss}}{\partial B} \rightarrow \frac{m_E}{d_E} \frac{\partial P_i}{\partial E}$) similar conditions emerge for positivity of the coefficients of the characteristic polynomial as in the *SDB* model (SI Sect. 2.3). Based on these similarities, we propose that the sufficient condition for stability found for the three-pool *SDB* model might also hold in the *SDBE* model. This proposed sufficient condition is given by

$$Z_{i \times j} = \left. \frac{\partial P_i}{\partial S} \right|_* + y_m f_D r_B d_B - y_m \left. \frac{m_E}{d_E} \frac{\partial P_i}{\partial E} \right|_* ; \quad Z_{i \times j} \geq 0 \quad (46)$$

The simplified causal loop diagram of the *SDBE* model in Fig. 2b gives rise to the same interpretation of this condition as in the *SDB* model. In the following we confirm that this condition holds in the *SDBE* model via numerical analysis.

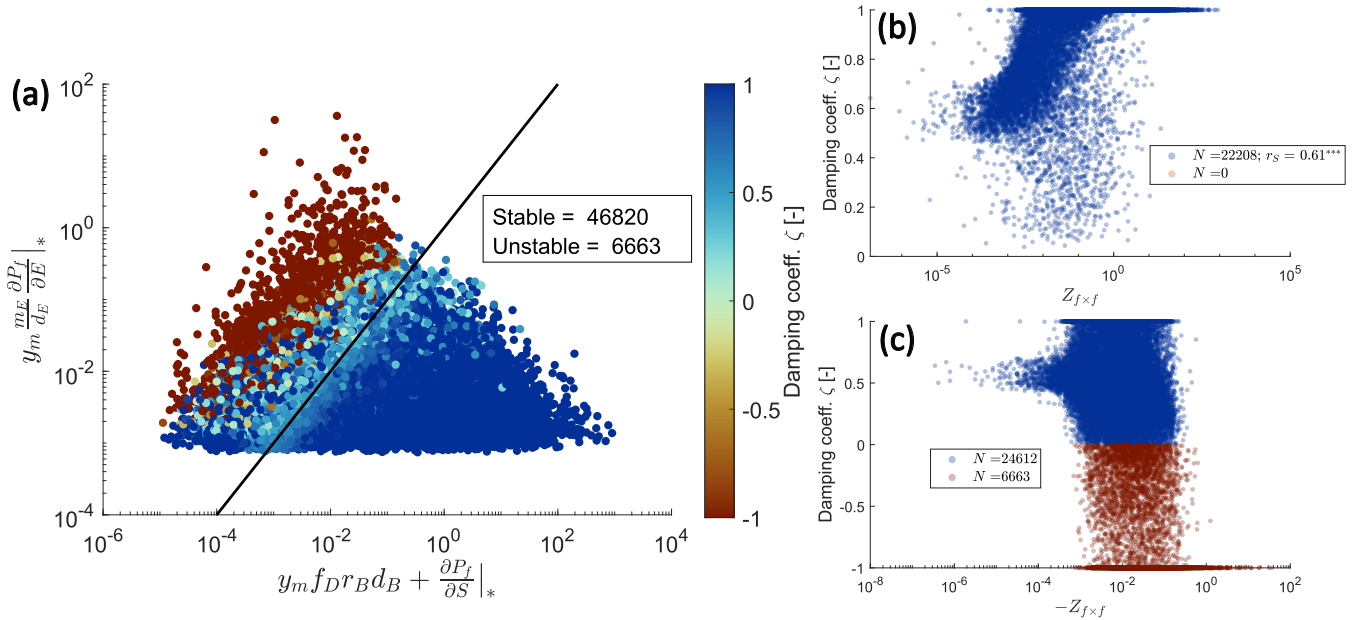


Figure 3. Numerical evaluation of the proposed sufficient condition for stability of the *SDBE* model with $f \times f$ kinetics and constitutive ENZ production. 100 000 Monte Carlo calculations of equilibrium points were produced sampling the parameter space in Table 3. (a) illustrates the separation of all physically meaningful equilibrium points by the positive and negative terms of $Z_{f \times f}$ (the proposed sufficient condition for stability, eq. 46). Points on and below the black 1:1 line (indicating $Z_{f \times f} = 0$) fulfill the condition $Z_{f \times f} \geq 0$. The color-code indicates the value of the damping coefficient ζ . (b) and (c) show values of ζ vs. values of $Z_{f \times f}$ (for $Z_{f \times f} \geq 0$ in (b), and $Z_{f \times f} < 0$ in (c)). Equilibrium points with $\zeta > 0$ or $\zeta \leq 0$ are marked with blue and red points, respectively; N gives the total number of equilibrium points in each category; r_s in (b) gives the Spearman rank correlation coefficient (***: significant at $p < 0.005$).

370 3.3.2 Numerical stability analysis

Testing the sufficient condition for stability

We produced 100 000 Monte Carlo simulations and computed the damping coefficient ζ (eq. 22) to numerically evaluate the stability of equilibrium points in the *SDBE* model. Within the sampled parameter space (Table 3), physically meaningful equilibrium points for which $Z_{i \times j} \geq 0$ (eq. 46) always also had $\zeta > 0$ and were thus stable (Fig. 3a-b, SI Fig. S1). Damping coefficients with $\zeta \leq 0$ were only observed when $Z_{i \times j} < 0$ (that is for points above the black line in Fig. 3a or red points in Fig. 3c). While a total of 46 820 evaluated equilibrium points were physically meaningful and stable, less than half of these (22 208) also fulfilled the condition $Z_{i \times j} \geq 0$. In turn, the majority of these equilibrium points (24 612) were stable despite contradicting this condition – i.e. the condition given by $Z_{i \times j} \geq 0$ is very conservative. In case the condition is fulfilled, the value of $Z_{i \times j}$ correlates well with the value of ζ meaning that for larger $Z_{i \times j}$ oscillations are generally more damped (Fig. 380 3b).

Changing environmental conditions, microbial physiology, and stability



Even for the simplified sufficient condition $Z_{i \times j} \geq 0$ analytical analysis is cumbersome for kinetics other than $m \times m$ (SI Sect. 2.3). We thus varied specific parameters individually and evaluated their effect on the numerically computed damping coefficient ζ .

385 Keeping all microbial and enzymatic parameters constant (set to their baseline value, that is for constitutive ENZ production, Table 3), stability depends on the environmental control parameters l_D and I (Fig. 4a). At baseline parameter values, most environmental conditions yield stable EPs but strong oscillations around these EPs occur (damping coefficient $\zeta < 1$). As conditions become less favourable and either l_D increases and/or I decreases, equilibrium points can become unstable ($\zeta < 0$).

Next, we analysed the influence of individual microbial parameter values on the stability of EPs for a number of scenarios defined by combinations of I and l_D (Fig. 4b-d; Table 7). Generally, if DOC leaching is neglected (solid lines, Fig. 4b-d), the variation in just one parameter rarely leads to unstable equilibria (only at very high microbial decay rates d_B). In contrast, if DOC leaching occurs, variation in key physiological parameters can lead to a transition from stable to unstable EPs. This happens as y_m becomes too low or d_B too high – i.e. for specific environmental conditions there are lower threshold values for y_m and upper thresholds for d_B beyond which equilibria become unstable (Fig. 4b-c, Table 7). With the exception of f_D , the partitioning of decayed microbial biomass between SOC and DOC, all parameters show such a threshold within the explored ranges (SI Fig. S2 and SI Sect. 2.3).

Using the alternative description of inducible production of extracellular enzymes, the stability behaviour with respect to changes in y_B is more varied (Fig. 4d). As for y_m , there are lower y_B threshold values below which steady states become unstable. However, there can also be upper thresholds for y_B above which too few enzymes are being produced to ensure sufficient C acquisition.

In summary, by varying only individual parameters, instabilities can arise when assimilation, depolymerization, or ENZ production are too low; or when abiotic C losses are too high (Fig. 4b-d; Fig. S2; Table 7). These results are in line with the analytic analysis of the sufficient condition (eq. 46) for $m \times m$ kinetics (SI Sect. 2.3).

Density-dependent mortality

405 Georgiou et al. (2017) proposed a density-dependent formulation of the microbial decay rate ($D_B^l = d_B^l B^b$ with $1 < b \leq 2$) as an alternative to the conventional linear decay term that yields mostly stable non-oscillatory behaviour (note that this formulation causes both microbial mortality and maintenance respiration to be density-dependent). For our *SDBE* model with DOC leaching, we could only find an analytical steady state solution for $m \times m$ kinetics and $b = 2$. In this case, the density dependent formulation could vastly alleviate the previously observed instability and resulted in damping coefficients for plausible equilibrium points close to 1 for most of the explored parameter spaces (SI Fig. S4a). However, some physically meaningful but unstable EPs were still observed. Only with negligible DOC leaching did physically meaningful but unstable equilibrium points vanish completely. This was numerically tested for $m \times m$, $f \times f$, and $r \times f$ kinetics (SI Fig. S4b-d).

Instability and predicted organic carbon pools

Fig. 5a-b illustrates the joint distributions of physically meaningful SOC and MBC pools in the $f \times f$ model for scenarios where DOC leaching is either considered (Fig. 5a) or neglected (Fig. 5b) (for 10 000 Monte Carlo simulations within the parameter ranges given in Table 3). By accounting for DOC leaching, just about half of the simulations yield physically

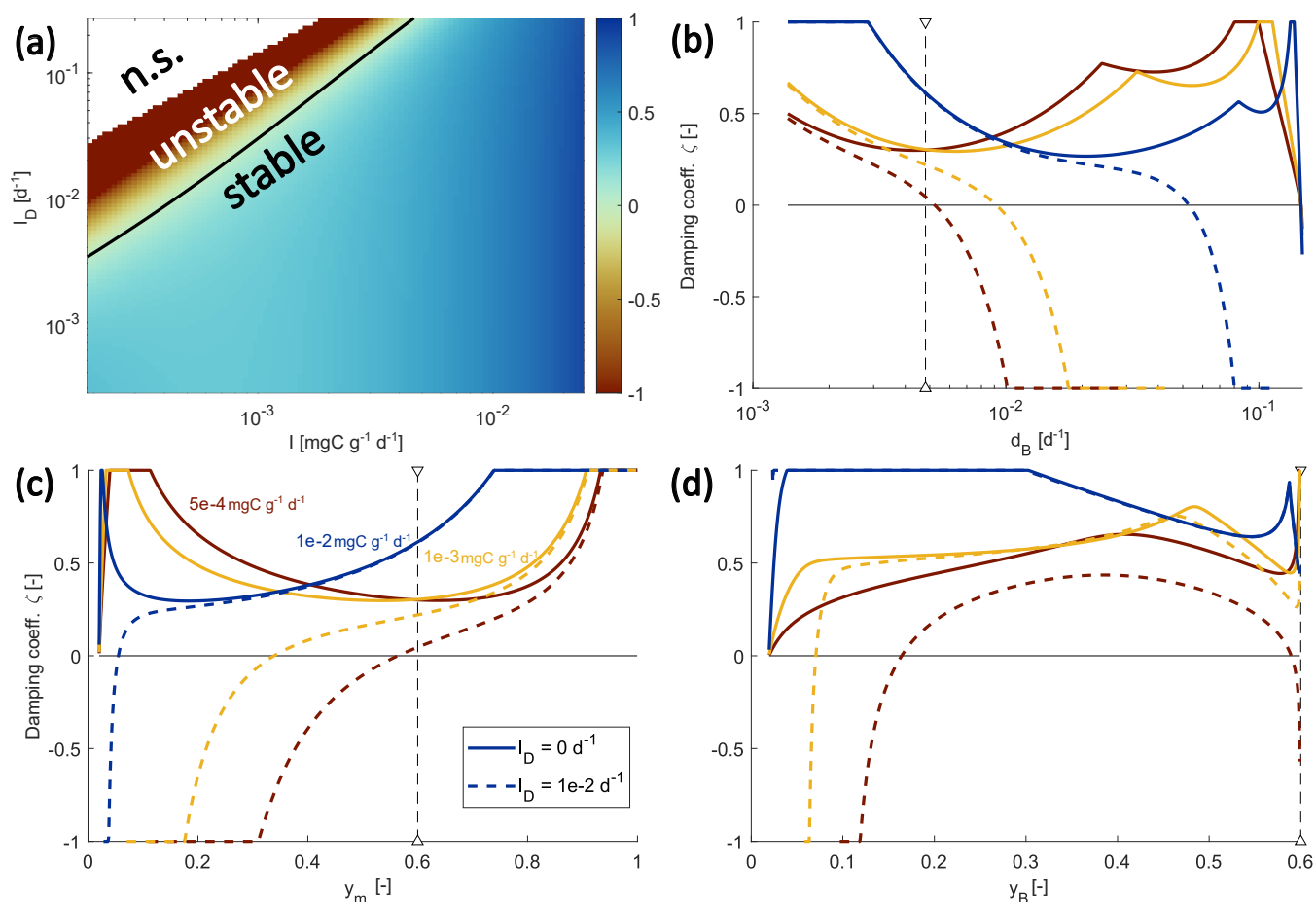


Figure 4. Changes in the damping coefficient with changes in environmental controls (a) and some microbial physiology parameters (b-d) in the *SDBE* model with $f \times f$ kinetics. (a) shows the dampening coefficient as a function of I and l_D with all other parameters held at their baseline values (Table 3). The black line indicates a $\zeta = 0$ (n.s. = no physically meaningful solution). (b-d) show variation in the damping coefficient for different combinations of I and l_D values. Different line styles indicate scenarios with different DOC leaching rate coefficients: solid lines indicate $l_D = 0$ and dashed lines $l_D = 1 \cdot 10^{-2}$. Different line colors indicate scenarios with different OC input rates: red lines indicate $I = 5 \cdot 10^{-4}$ mgC g⁻¹ d⁻¹, yellow lines $I = 1 \cdot 10^{-3}$ mgC g⁻¹ d⁻¹, and dark blue lines $I = 1 \cdot 10^{-2}$ mgC g⁻¹ d⁻¹. In (b) and (c) the baseline model with constitutive production of extracellular enzymes is used and d_B and y_m varied respectively. Baseline parameter values are indicated by vertical dashed lines. In (d) instead only inducible production of extracellular enzymes is considered and y_B varied. Note the log x- and y-axis in panel (a) and the log x-axis in panel (b).



Table 7. Indication of thresholds in parameter values for stability of the *SDBE* model. Analysis is based on exclusively varying one parameter while keeping all others at their baseline value (Table 3; Fig. 4, SI Fig. S2). Analysis applies to all evaluated combinations of kinetics ($m \times m$, $f \times f$, $r \times f$) using constitutive ENZ production; except for analysis of y_B where we considered only inducible ENZ production. ($i = m, f, r$), ($j = m, f$).

Process	Parameter	Threshold		
		Lower	Upper	None
Depolymerization	v_i^p	X		
	K_i^p		X	
Assimilation	v_j^u	X		
	K_f^u		X	
	y_m	X		
ENZ production	m_E	X		
	y_B	X	X	
Decay	d_B		X	
	d_E		X	
Mass balance losses	r_B	X		
	l_D		X	
OC Input	I	X		
SOC-DOC partition	f_I		X	
	f_D			X

420 meaningful EPs – of which most (4 698) were also stable, but more than 10 % (687) were unstable. Neglecting DOC leaching increases the total number of physically meaningful results (6 896) and simultaneously reduces the relative share of physically meaningful but unstable results to < 5 % (312). In both scenarios, most simulations yield implausible results for steady state C
 425 stocks – e.g. MBC being larger than SOC. However, in both scenarios, unstable EPs largely overlap with stable and plausible outcomes in the SOC-MBC solution space. This is also evident in the empirical probability density functions of all the four state variables (Fig. 5c-d). Especially if DOC leaching is considered ($l_D > 0$, Fig. 5c), values of plausible and unstable steady state SOC pools largely overlap. In contrast, the distributions of plausible and unstable steady state pool sizes of MBC, DOC, and ENZ do not overlap as closely as those for SOC. These distinctions are amplified in the cases where DOC leaching is neglected ($l_D = 0$, Fig. 5d), in particular for DOC.

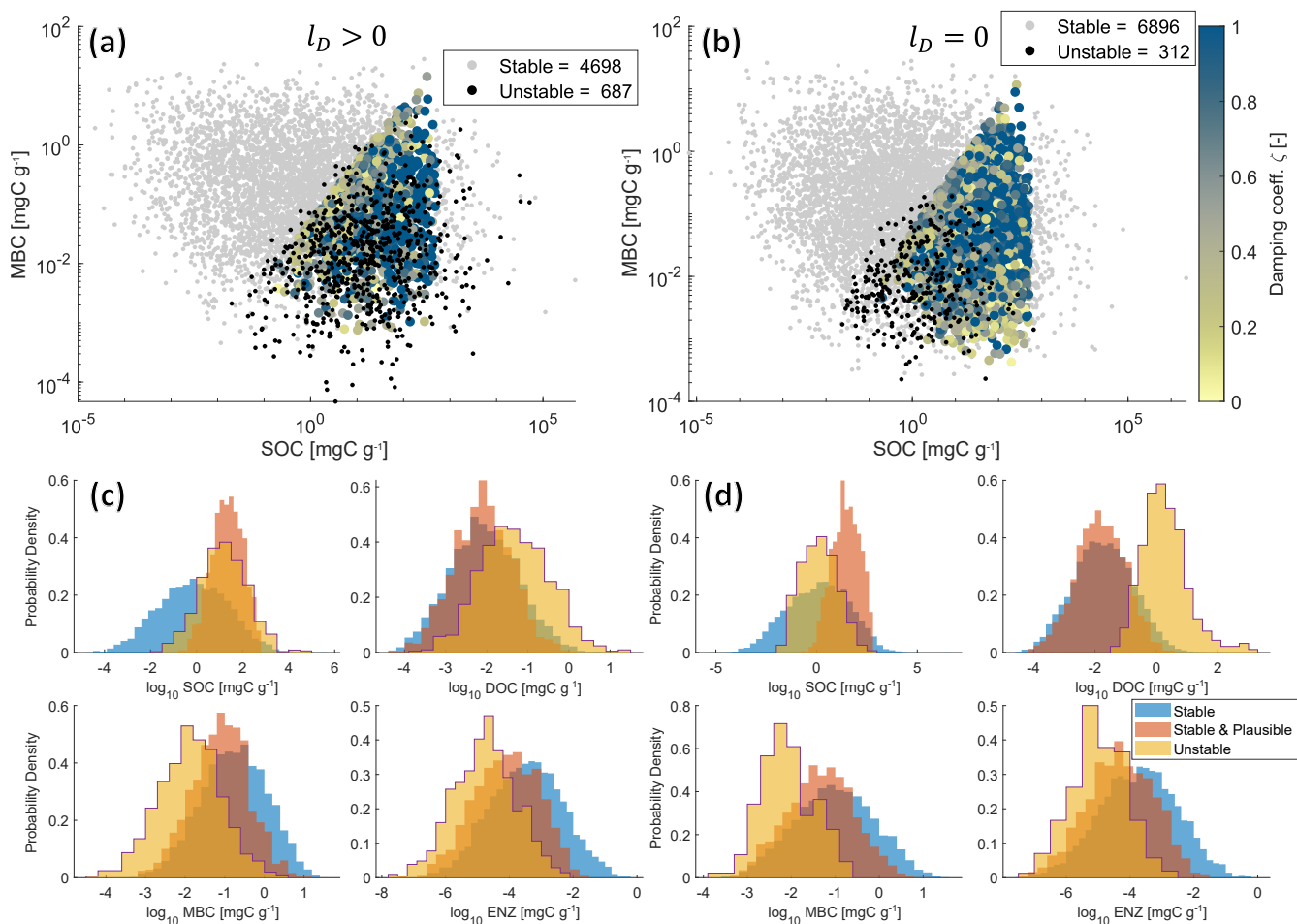


Figure 5. Physically meaningful (positive & real) steady state solutions from 10 000 Monte Carlo simulations of the *SDBE* model with $f \times f$ kinetics and constitutive ENZ production. Scatter plots of MBC vs. SOC concentrations are shown for $l_D > 0$ (a) and $l_D = 0$ (b). Grey points are stable steady state solutions, color-coded points are stable steady state solutions yielding plausible results, and black points are physically meaningful but unstable steady state solutions. The color code indicates the value of the damping coefficient. Legends indicate the numbers of physically meaningful and stable (stable + stable & plausible) or unstable EPs. Plot groups (c) and (d) show empirical probability density functions of each state variable for stable, stable & plausible, and unstable physically meaningful steady state solutions for $l_D > 0$ and $l_D = 0$, respectively. Note that SOC contents $> 1000 \text{ mg C g}^{-1}$ are mathematically possible but unphysical model outcomes, as we neglect soil volume changes.



4 Discussion

4.1 Model structure matters: standard microbial-explicit SOC models can have unstable equilibria

Manzoni and Porporato (2007) and Raupach (2007) showed analytically that the non-trivial steady state of two-pool models, consisting of a substrate pool and a microbial pool (respectively a “harvester” system in Raupach, 2007), are always stable for
430 multiplicative and forward Michaelis-Menten kinetics (but only under the assumption that the input to the substrate (I) is a constant; Raupach, 2007). We show here that the same is true for all physically meaningful, non-trivial (“biotic”) equilibrium points also if a third pool representing extracellular enzymes is added (SBE model). This result holds irrespective of the kinetic laws used to describe SOC depolymerization and whether ENZ production is considered to be constitutive, inducible, or a combination of both.

435 Interestingly, by introducing a second non-linear term Raupach (2007) found that unstable equilibria could emerge in their two-pool model. In contrast, Wang et al. (2014, 2016) demonstrated for several versions of a three-pool (litter-SOC-microbes) model with two non-linearities (microbial degradation and subsequent uptake of litter and SOC) that the equilibrium points of these models were always stable. An underlying assumption in these models was that the available substrate pool (similar to what we described as DOC) was at quasi-steady state. Our derivation of the SBE model follows a similar simplification –
440 and also does not yield unstable behaviour. By contrast, unstable equilibrium points are possible in our three- and four-pool model versions with two non-linearities that explicitly consider DOC (SDB and $SDBE$ model). Whether equilibrium points in microbial-explicit SOC models can become unstable is thus not dependent on the number of pools or the number of non-linearities *per se*, but rather on the combination of non-linearities, the coupling of different pools and rates, and what feedbacks they create.

445 Comparing our three- and four-pool models to the simpler two-pool model analysed by Raupach (2007) can help to understand why instability can occur in these models. Briefly, their model describes human consumption of a food resource, but is in structure similar to our models (analogous terms in our models are given in brackets): the resource (SOC in SBE , DOC in SDB and $SDBE$ models), is taken up by the human consumer (microbes), and thereby depleted. The uptake process is always described as a non-linear term, equivalent to our description of U_j . Raupach (2007) analysed two different cases with
450 respect to the resupply of the resource (I in SBE , $(1 - f_I)I + P_i^\dagger$ in SDB and $SDBE$): 1) resupply is independent of the available resource and 2) resupply is dependent on the resource itself. The first case is similar to our SBE model, where the resource SOC is replenished only by the external input I and is thus completely independent of the SOC availability itself. In these cases the “biotic” (respectively resource-human coexistence in Raupach, 2007) equilibrium is always stable if it is physically meaningful. In turn, the second case can be compared to our SDB and $SDBE$ models: unless the external input to
455 DOC is very high (for low f_I), the replenishment of the resource DOC is dominated by the depolymerization rate P_i^\dagger – which via the positive feedback loop R_1 is dependent on the available DOC (compare Fig. 2b). These models can have unstable “biotic” equilibria (Raupach, 2007). Therefore, the (more or less direct) dependency of the resource resupply on the abundance of the resource itself can be identified as the root cause that allows for instability in these models.



We further tested this hypothesis by setting $f_I = 0$ in the *SDBE* model (i.e., all external input goes into DOC directly),
460 bypassing the dependency of DOC replenishment on depolymerization. In line with our expectation (and the analytical solution
of $Z_{m \times m}$ and $Z_{f \times f}$ for $f_I = 0$ in SI Sect. 2.3) this effectively prevented the occurrence of unstable EPs (SI Fig. S5).

4.2 Avoiding instability

Our analysis of different model structures and their stability behaviour points to three direct approaches to avoid unstable EPs
in microbial-explicit SOC models:

- 465
1. model structure – avoid positive feedback coupling between microbial growth substrate (here DOC) available for uptake
and its resupply
 2. kinetic formulations – avoid accelerated depletion of DOC by reducing the dependency of uptake on microbial biomass
 3. parameter values – choose parameter values so that the sufficient and/or necessary conditions for stability are met.

The first approach is commonly taken in models that assume DOC to be in quasi-steady state (e.g. Wang et al., 2014, 2016),
470 but might have shortcomings in cases where DOC dynamics become important e.g. if drying-rewetting dynamics or leaching
are relevant. If DOC leaching is not considered to be a relevant process, neglecting this process but keeping a dynamic
description of DOC can already considerably reduce the likelihood of unstable EPs.

The second approach is used e.g. in models that assume DOC uptake as independent of microbial biomass, but dependent
on the availability of DOC respectively its diffusive flux to a cell (e.g. Manzoni et al., 2014). Alternatively, using for instance
475 reverse Michaelis-Menten kinetics to describe microbial uptake can dampen oscillations (Wang et al., 2016). Since uptake
kinetics using reverse Michaelis-Menten or the ECA formulation become similar to linear uptake kinetics at relatively high
concentrations of microbial biomass they could also help to alleviate instability issues under these conditions.

Lastly, the third approach might seem straight forward as we could expect parameter values calibrated with measurement
data to yield both stable and plausible EPs. However, our numerical simulations indicated that especially if DOC leaching is
480 considered, calibrating parameter values with SOC and microbial biomass data alone could still lead to plausible yet unsta-
ble EPs (Fig. 5). While data on carbon contents in the extracellular enzyme pool are still not available, combining microbial
biomass data with quantitative data on DOC pools (as e.g. in Wang et al., 2013) could help to avoid calibration to parameter val-
ues that lead to unstable EPs. Moreover, stability criteria can be obeyed in various other ways, e.g. by considering correlations
between parameter values or introducing additional constraints on microbial physiology.

485 4.2.1 Correlations between parameter values

Correlations between parameter values could effectively alleviate the occurrence of unstable EPs by simultaneously changing
parameter values that appear on both sides of the inequality given by eq. 43 or 46, thereby ensuring that these conditions are
always fulfilled even as parameter values change. Some evidence for this to be effective is provided e.g. by Hararuk et al. (2015),
who used the four-pool AWB model (Allison et al., 2010) (similar to the *SDBE* model) for predictions of global carbon stocks.



490 They prescribed e.g. the uptake and depolymerization rate coefficients and the respective half-saturation constants to positively correlate with temperature. Thus, with the same directional change in temperature, these parameter values change in opposite directions with respect to their threshold values for stability (Table 7) – i.e., with a decrease in temperature v_f^p decreases, moving closer to its threshold, but simultaneously also K_f^p decreases, moving further away from its threshold. Consequently, for a wide range of parameter values the conditions for stability could be fulfilled. Indeed, Hararuk et al. (2015) reported that
495 they did not observe any unstable equilibria with maximum-likelihood parameters in their global study.

Beyond the qualitative assessment of parameter thresholds (Table 7), explicit analytical expressions of the necessary or sufficient conditions for stability (as for $Z_{m \times m}$ in SI Sect. 2.3) could be used to quantitatively assess what parameter correlations are required to ensure stability of equilibria across reasonable parameter ranges. However, for other kinetic formulations than $m \times m$ these terms might become difficult to trace analytically.

500 4.2.2 Constraints on microbial physiology

The observation of stability thresholds of parameters moving as environmental conditions are changing can further be interpreted in the light of expected variations in microbial functional traits. While some kinetic rate parameters might be correlated due to thermodynamics (e.g. temperature response of rate parameters), correlations among other parameters, like the investment into growth or extracellular enzyme production, might rather emerge as outcomes of eco-evolutionary processes that
505 select specific combination of traits in a given environment (Abs et al., 2023). These combinations of traits would manifest themselves as microbial life-history strategies under different environmental conditions (e.g. Malik et al., 2020). Following this logic, changing environmental conditions could constrain the space for microbial physiological adaptation because microbial traits would need to ensure stability. For example, very inefficient microbes (having a low y_m) could not establish a stable equilibrium under very unfavourable conditions (low OC input and/or high DOC leaching, Fig. 4c) – unless other traits change
510 simultaneously. This reflects a basic principle of ecology: that organisms have to be adapted to the environment they inhabit. Currently, this basic principle is not integrated in microbial-explicit SOC models (but see Abs et al., 2022, for a recent attempt at addressing this challenge), which can lead to matching specific environmental conditions with a (modelled) microbial population that is not able to sustain itself under those conditions.

Integrating soil microbial ecological understanding into microbial-explicit SOC models could instead yield alternative mathematical descriptions or parameter relations that could prevent such mismatching, and ultimately improve model applicability
515 (Georgiou et al., 2017). Evidence on the importance of microbial ecology and evolution for SOC cycling is accumulating (Abs et al., 2022, 2023). For instance, microbes have been found to invest more into production of extracellular enzymes in soils with lower SOC contents (Calabrese et al., 2022; Malik et al., 2019) and density-dependent microbial mortality, a concept derived from ecological considerations, can effectively alleviate oscillatory behaviour (Georgiou et al., 2017).

520 The most noticeable difference between these approaches to avoiding instability in microbial-explicit SOC models might be whether they globally avoid occurrence of unstable equilibria (e.g., by not explicitly representing DOC), or whether they constrain the available parameter spaces so that for reasonable parameter values instability is avoided (e.g. by introducing parameter correlations or additional balancing mechanisms). As different research questions require different models, there is



no clear answer to which of these approaches should be preferred. However, in line with Abs et al. (2022, 2023) and Georgiou
525 et al. (2017) we want to highlight the potential of using ecologically consistent mathematical descriptions to improve current
model formulations. In other words, we cannot simply add a biotic component to models without acknowledging that this
component has to be “adapted” (as species and communities are in the real world) to the environmental conditions it is exposed
to.

4.3 Relevance for model applications

530 Our numerical analysis of the *SDBE* model indicates that instability of equilibrium points becomes more likely with decreasing
carbon inputs, increasing DOC leaching, and low process rates (Fig. 4, Table 7). All these conditions are most likely to be
met in high altitude and/or latitude environments. This is in line with Hararuk et al. (2015), who observed strongest oscillations
(longest time to dampen oscillations, indicative of diminishing real parts of the eigenvalues) of their calibrated four-pool
model in these regions. Therefore, analytical steady states of microbe-explicit SOC models applied in high altitude and/or
535 latitude environments could be unstable and analytical steady state solutions could thus not reliably be used for initialization
of simulation runs or prediction of SOC stocks.

We could identify a sufficient and necessary condition for stability of the *SDB* model (eq. 39-41). However, the condition
we found is difficult to interpret and apply. We thus proposed a stricter but simpler sufficient condition for stability (eq. 43).
By comparing the *SDB* and *SDBE* model we proposed that a similar constraint ($Z_{i \times j} \geq 0$, eq. 46) would also hold as a
540 sufficient condition for the *SDBE* model, despite the Routh-Hurwitz stability criterion being not fully tractable analytically
for this model version. Numerical analyses confirmed that the proposed sufficient condition ensures stability of the *SDBE*
model within the vast parameter space we explored. However, these sufficient conditions are very conservative and can exclude
a substantial fraction of the physically meaningful and stable equilibrium points. Further, despite a clear correlation between
 $Z_{i \times j}$ and the damping coefficient ζ , the stability condition does not give direct insights into the oscillation behaviour. How
545 useful the stricter sufficient and necessary conditions would be in constraining model parameters – as compared to the simpler
sufficient conditions – might depend on the specific model applications. Despite the potential challenges in evaluating these
conditions, they can still be useful to understand the processes or parameter interactions that cause unstable EPs to occur and
can guide ecology-informed model developments.

5 Conclusions

550 Microbial-explicit SOC models aim to improve the representation of SOC dynamics by accounting for its biotic control. By
this, even simple archetypal models can describe a multitude of relevant processes and varied dynamics. At very small spatial
and temporal scales their oscillatory behaviour and potential for instability can reflect relevant (micro-)ecosystem processes
(Manzoni and Porporato, 2007). However, if applied at larger scales such as in Earth-system models, these properties can
result in unrealistic simulation outcomes (Georgiou et al., 2017; Wang et al., 2014). Here we analyzed what processes can
555 lead to instability in these models. By comparing the stability behaviour of an archetypal microbial-explicit SOC model with



some reduced model versions and stability analysis of similar models in the literature, we found that instability can occur in models that assume a positive feedback between the resupply of a microbial growth substrate (i.e. DOC) and its abundance. We found that stability is (sufficiently) conditional on the balance between the sensitivity of the depolymerization rate to changes in extracellular enzyme vs. SOC concentration. Based on these analyses, we suggest that instability can be avoided by
560 selecting specific 1) model structures, 2) kinetic formulations, and/or 3) parameter relations or values. While these approaches can vastly differ, an emerging common theme is that acknowledging ecological principles and processes can be leveraged to improve model applicability.

Author contributions. ES and SM conceptualized the study. ES and SG lead and SM and SB assisted the formal analysis and investigation. All authors discussed results together. ES wrote the original manuscript draft and produced the figures. SM gave continuous feedback
565 throughout the manuscript writing. All authors reviewed and commented on the manuscript draft.

Competing interests. The authors declare that they have no conflict of interest.

Acknowledgements. We thank Björn Lindahl for inspiring discussions and valuable comments on the manuscript. ES and SM were funded by the European Research Council (ERC) under the European Union's Horizon 2020 Research and Innovation Programme (grant agreement no 101001608). SG was funded by Swedish Research Council Vetenskapsrådet (grant no 2020-03910) and the Swedish Research Council
570 FORMAS (grant 2021-02121).



References

- Abs, E., Saleska, S., and Ferriere, R.: Microbial eco-evolutionary responses amplify global soil carbon loss with climate warming, *Research Square* [preprint], <https://doi.org/10.21203/rs.3.rs-1984500/v1>, 2022.
- Abs, E., Chase, A. B., and Allison, S. D.: How do soil microbes shape ecosystem biogeochemistry in the context of global change?, *Environmental Microbiology*, 25, 780–785, <https://doi.org/10.1111/1462-2920.16331>, 2023.
- Allison, S. D., Wallenstein, M. D., and Bradford, M. A.: Soil-carbon response to warming dependent on microbial physiology, *Nature Geoscience*, 3, 336–340, <https://doi.org/10.1038/ngeo846>, 2010.
- Argyris, J. H., Faust, G., Haase, M., and Friedrich, R.: *An Exploration of Dynamical Systems and Chaos: Completely Revised and Enlarged Second Edition*, Springer Berlin, Heidelberg, ISBN 978-3-662-46042-9, <https://doi.org/10.1007/978-3-662-46042-9>, 2015.
- Bradford, M. A., Wieder, W. R., Bonan, G. B., Fierer, N., Raymond, P. A., and Crowther, T. W.: Managing uncertainty in soil carbon feedbacks to climate change, *Nature Climate Change*, 6, 751–758, <https://doi.org/10.1038/nclimate3071>, 2016.
- Calabrese, S., Mohanty, B. P., and Malik, A. A.: Soil microorganisms regulate extracellular enzyme production to maximize their growth rate, *Biogeochemistry*, 158, 303–312, <https://doi.org/10.1007/s10533-022-00899-8>, 2022.
- Chakrawal, A., Calabrese, S., Herrmann, A. M., and Manzoni, S.: Interacting Bioenergetic and Stoichiometric Controls on Microbial Growth, *Frontiers in Microbiology*, 13, 859 063, <https://doi.org/10.3389/fmicb.2022.859063>, 2022.
- Cotrufo, M. F. and Lavelle, J. M.: Soil organic matter formation, persistence, and functioning: A synthesis of current understanding to inform its conservation and regeneration, vol. 172 of *Advances in Agronomy*, pp. 1–66, Academic Press, ISBN 978-0-323-98953-4, <https://doi.org/10.1016/bs.agron.2021.11.002>, 2022.
- Georgiou, K., Abramoff, R. Z., Harte, J., Riley, W. J., and Torn, M. S.: Microbial community-level regulation explains soil carbon responses to long-term litter manipulations, *Nature Communications*, 8, 1223, <https://doi.org/10.1038/s41467-017-01116-z>, 2017.
- Haraldsson, H. V.: *Introduction to System Thinking and Causal Loop Diagrams*, Lund University, Department of Chemical Engineering, 2004.
- Hararuk, O., Smith, M. J., and Luo, Y.: Microbial models with data-driven parameters predict stronger soil carbon responses to climate change, *Global Change Biology*, 21, 2439–2453, <https://doi.org/10.1111/gcb.12827>, 2015.
- Horn, R. A. and Johnson, C. R.: *Topics in Matrix Analysis*, Cambridge University Press, 1991.
- Malik, A. A., Puissant, J., Goodall, T., Allison, S. D., and Griffiths, R. I.: Soil microbial communities with greater investment in resource acquisition have lower growth yield, *Soil Biology and Biochemistry*, 132, 36–39, <https://doi.org/10.1016/j.soilbio.2019.01.025>, 2019.
- Malik, A. A., Martiny, J. B. H., Brodie, E. L., Martiny, A. C., Treseder, K. K., and Allison, S. D.: Defining trait-based microbial strategies with consequences for soil carbon cycling under climate change, *The ISME Journal*, 14, 1–9, <https://doi.org/10.1038/s41396-019-0510-0>, 2020.
- Manzoni, S. and Porporato, A.: A theoretical analysis of nonlinearities and feedbacks in soil carbon and nitrogen cycles, *Soil Biology and Biochemistry*, 39, 1542–1556, <https://doi.org/10.1016/j.soilbio.2007.01.006>, 2007.
- Manzoni, S. and Porporato, A.: Soil carbon and nitrogen mineralization: Theory and models across scales, *Soil Biology and Biochemistry*, 41, 1355–1379, <https://doi.org/10.1016/j.soilbio.2009.02.031>, 2009.
- Manzoni, S., Schaeffer, S., Katul, G., Porporato, A., and Schimel, J.: A theoretical analysis of microbial eco-physiological and diffusion limitations to carbon cycling in drying soils, *Soil Biology and Biochemistry*, 73, 69–83, <https://doi.org/10.1016/j.soilbio.2014.02.008>, 2014.



- Raupach, M. R.: Dynamics of resource production and utilisation in two-component biosphere-human and terrestrial carbon systems, *Hydrology and Earth System Sciences*, 11, 875–889, <https://doi.org/10.5194/hess-11-875-2007>, 2007.
- 610 Richardson, G. P.: Problems with causal-loop diagrams, *System Dynamics Review*, 2, 158–170, <https://doi.org/10.1002/sdr.4260020207>, 1986.
- Schimel, J. P. and Weintraub, M. N.: The implications of exoenzyme activity on microbial carbon and nitrogen limitation in soil: a theoretical model, *Soil Biology and Biochemistry*, 35, 549–563, [https://doi.org/10.1016/S0038-0717\(03\)00015-4](https://doi.org/10.1016/S0038-0717(03)00015-4), 2003.
- Sierra, C. A. and Müller, M.: A general mathematical framework for representing soil organic matter dynamics, *Ecological Monographs*, 85, 615 505–524, <https://doi.org/10.1890/15-0361.1>, 2015.
- Tang, J. and Riley, W. J.: Competitor and substrate sizes and diffusion together define enzymatic depolymerization and microbial substrate uptake rates, *Soil Biology and Biochemistry*, 139, 107–124, <https://doi.org/10.1016/j.soilbio.2019.107624>, 2019.
- Tang, J. Y. and Riley, W. J.: A total quasi-steady-state formulation of substrate uptake kinetics in complex networks and an example application to microbial litter decomposition, *Biogeosciences*, 10, 8329–8351, <https://doi.org/10.5194/bg-10-8329-2013>, 2013.
- 620 Tao, F., Huang, Y., Hungate, B. A., Manzoni, S., Frey, S. D., Schmidt, M. W. I., Reichstein, M., Carvalhais, N., Ciais, P., Jiang, L., Lehmann, J., Wang, Y.-P., Houlton, B. Z., Ahrens, B., Mishra, U., Hugelius, G., Hocking, T. D., Lu, X., Shi, Z., Viatkin, K., Vargas, R., Yigini, Y., Omuto, C., Malik, A. A., Peralta, G., Cuevas-Corona, R., Di Paolo, L. E., Luotto, I., Liao, C., Liang, Y.-S., Saynes, V. S., Huang, X., and Luo, Y.: Microbial carbon use efficiency promotes global soil carbon storage, *Nature*, 618, 981–985, <https://doi.org/10.1038/s41586-023-06042-3>, 2023.
- 625 The MathWorks Inc.: MATLAB version: 9.13.0.2105380 (R2022b) Update 2, Tech. rep., Natick, Massachusetts, United States, <https://www.mathworks.com>, 2022.
- Todd-Brown, K. E. O., Randerson, J. T., Post, W. M., Hoffman, F. M., Tarnocai, C., Schuur, E. A. G., and Allison, S. D.: Causes of variation in soil carbon simulations from CMIP5 Earth system models and comparison with observations, *Biogeosciences*, 10, 1717–1736, <https://doi.org/10.5194/bg-10-1717-2013>, 2013.
- 630 Varney, R. M., Chadburn, S. E., Burke, E. J., and Cox, P. M.: Evaluation of soil carbon simulation in CMIP6 Earth system models, *Biogeosciences*, 19, 4671–4704, <https://doi.org/10.5194/bg-19-4671-2022>, 2022.
- Wang, G., Post, W. M., and Mayes, M. A.: Development of microbial-enzyme-mediated decomposition model parameters through steady-state and dynamic analyses, *Ecological Applications*, 23, 255–272, <https://doi.org/10.1890/12-0681.1>, 2013.
- Wang, G., Jagadamma, S., Mayes, M. A., Schadt, C. W., Megan Steinweg, J., Gu, L., and Post, W. M.: Microbial dormancy improves 635 development and experimental validation of ecosystem model, *The ISME Journal*, 9, 226–237, <https://doi.org/10.1038/ismej.2014.120>, 2015.
- Wang, Y. P., Chen, B. C., Wieder, W. R., Leite, M., Medlyn, B. E., Rasmussen, M., Smith, M. J., Augusto, F. B., Hoffman, F., and Luo, Y. Q.: Oscillatory behavior of two nonlinear microbial models of soil carbon decomposition, *Biogeosciences*, 11, 1817–1831, <https://doi.org/10.5194/bg-11-1817-2014>, 2014.
- 640 Wang, Y. P., Jiang, J., Chen-Charpentier, B., Augusto, F. B., Hastings, A., Hoffman, F., Rasmussen, M., Smith, M. J., Todd-Brown, K., Wang, Y., Xu, X., and Luo, Y. Q.: Responses of two nonlinear microbial models to warming and increased carbon input, *Biogeosciences*, 13, 887–902, <https://doi.org/10.5194/bg-13-887-2016>, 2016.
- Wieder, W. R., Bonan, G. B., and Allison, S. D.: Global soil carbon projections are improved by modelling microbial processes, *Nature Climate Change*, 3, 909–912, <https://doi.org/10.1038/nclimate1951>, 2013.



- 645 Wieder, W. R., Grandy, A. S., Kallenbach, C. M., and Bonan, G. B.: Integrating microbial physiology and physio-chemical principles in soils with the MIcrobial-MIneral Carbon Stabilization (MIMICS) model, *Biogeosciences*, 11, 3899–3917, <https://doi.org/10.5194/bg-11-3899-2014>, 2014.
- Wieder, W. R., Allison, S. D., Davidson, E. A., Georgiou, K., Hararuk, O., He, Y., Hopkins, F., Luo, Y., Smith, M. J., Sulman, B., Todd-Brown, K., Wang, Y., Xia, J., and Xu, X.: Explicitly representing soil microbial processes in Earth system models, *Global Biogeochemical Cycles*, 29, 1782–1800, <https://doi.org/10.1002/2015GB005188>, 2015.
- 650 Wieder, W. R., Hartman, M. D., Sulman, B. N., Wang, Y., Koven, C. D., and Bonan, G. B.: Carbon cycle confidence and uncertainty: Exploring variation among soil biogeochemical models, *Global Change Biology*, 24, 1563–1579, <https://doi.org/10.1111/gcb.13979>, 2018.